Development of a clean and energy self-sustained building in the vision of integrating H2 economy with renewable energy sources

Deliverable D9.2
Performance evaluation of the full scale prototype

Document Details

Due date of Deliverable:	30-09-2012
Lead Contractor for Deliverable:	NTUA and CRES
Dissemination Level (*):	CO
Revision:	0
Preparation Date:	30-11-2012
Prepared by:	Panorios Benardos, Antonis Peppas, Lampros Karalis
Verified by:	Antonis Peppas
Internal Ref. No.	

(*) *Only one choice between CO (Consortium), CR (Partners Concerned), PU (Public)*

Project Contractual Details

Project Title:	Development of a clean and energy self-sustained building in the vision of integrating H_2 economy with renewable energy sources
Project Acronym:	H2SusBuild
Grant Agreement No.:	NMP2-LA-2008-214395
Project Start Date:	01-10-2008
Project End Date:	30-09-2012
Duration:	48 months

Supplementary notes:
This document is only for use among the Partners of H2SusBuild

TABLE OF CONTENTS

1. INTRODUCTION

The present document constitutes Deliverable D9.2 in the framework of the H2SusBuild project titled “Development of a clean and energy self-sustained building in the vision of integrating H_2 economy with renewable energy sources” (Project Acronym: H2SusBuild; Contract No.: FP7-NMP2-LA-2008-214395).

This report describes the activities performed within the framework of WP9 “Scaling up and development of an integrated RES-H_2 full-scale demonstrator” that refers to the results from the installation and operation of the full-scale system and the evaluation of its performance.

Additionally, the report contains all relevant information regarding the full-scale prototype system technical specifications, description of maintenance activities carried out (where needed) and problems encountered during operation, lessons learned during the installation and operation phases of the project, as well as recommendations for future component and/or system optimizations. In this context, a series of activities for the optimization of the full-scale system control algorithm that were performed cooperatively by NTUA and IKERLAN is discussed.

The report also presents the final version of the manual for the proper and safe operation and maintenance of the system, which has been updated with information concerning the full-scale system and the new features and functionalities that have been added during and after the scaling up activities.

2. SCALING UP ACTIVITIES

The small-scale pilot prototype plant aimed at integrating individual components of the RES-H_2 system in order to verify the synergistic operation between them and evaluate the system viability, efficiency and safety through monitoring and data gathering. During the development of the small-scale prototype plant, emphasis was placed on completing in advance construction works and equipment installation that would also be required for the full-scale installation so as to minimize the required work during the second phase of the project.

Therefore, comparing the small-scale and full-scale prototype plants in terms of equipment, the newly installed components include:

- The 20 kWe micro-CHP FC and its peripherals
- The prototype H_2 burner and the condensing boiler
- The H_2 compressor
- Additional pressure cylinder stacks for increased storage capacity
- The Heat Recovery System (HRS)

In Figure 1, the final as-built placement of all components in the GenConStore area is presented. The components that were installed during the small-scale phase are shown with yellow color, while the full-scale installed and/or modified components are shown with orange color.

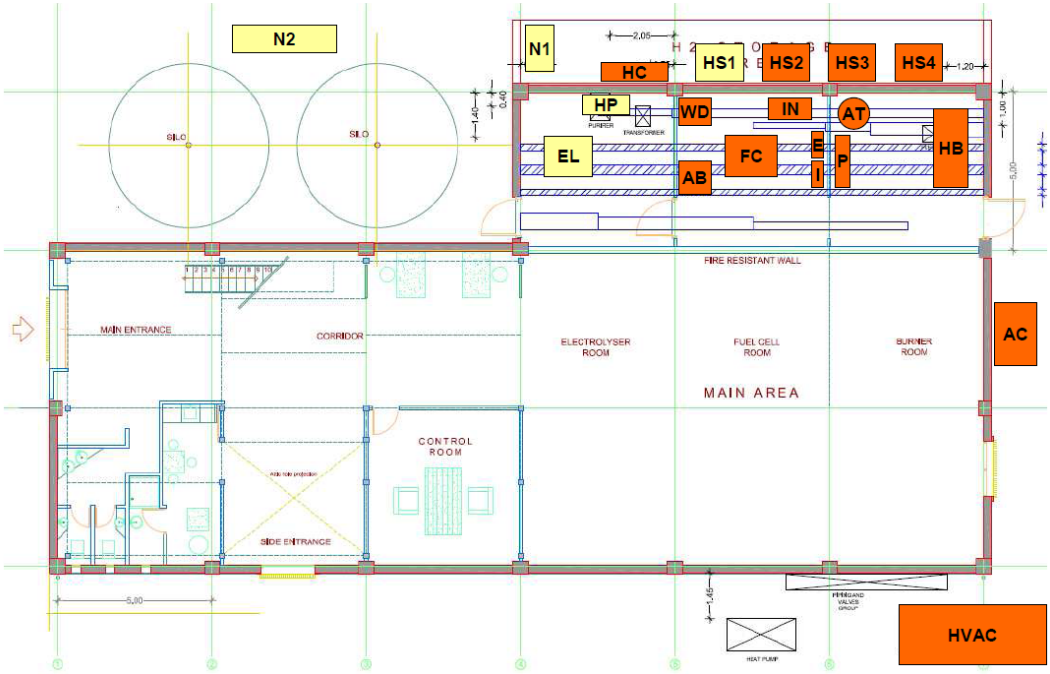

Figure 1. As-built full-scale prototype plant installation.

2.1 Micro-CHP

The micro-CHP and its peripherals were developed and supplied by ICI Caldaie, while NTUA was in responsible for preparing the demonstration building infrastructure for the installation and integration of the equipment. The components were installed in the Fuel Cell Room (FCR) as originally planned. The peripherals of the micro-CHP include:

- Air blower that filters the atmospheric air and supplies it to the micro-CHP
- Air to water cooler for the cooling of the micro-CHP (installed outside the building)
- Water deionization system
- DC/AC 3-phase inverter
- Control cabinet including a software PLC

The scaling up activities included:

- Civil works to allow for upgraded ventilation of the FCR and venting from the micro-CHP
- Piping installation for connecting the municipal water grid to the water deionization system, for hydraulic connection with the HRS and for water drainage towards the building's exterior
- H_2 grid modifications with upgraded pressure regulators and relief valves as well as new piping for the supply of H_2 to the micro-CHP and for venting
- Electrical modifications for the integration of the control cabinet and the 3-phase inverter as well as cabling for connection with the HRS
- Modifications to the EMCS programming logic in order to integrate the micro-CHP FC to the existing small-scale RES-H_2 system

The micro-CHP FC and some of its peripherals can be seen in Figure 2.

Figure 2. From left to right: a) Micro-CHP FC, b) inverter and c) Control cabinet.

2.2 H_2 Burner

Similar to the micro-CHP, the prototype H_2 burner (Figure 3) was also developed and supplied by ICI Caldaie while NTUA was responsible for preparing the demonstration building infrastructure for the installation and integration of the equipment. The burner and the accompanying condensing boiler were installed in the Burner Room (BR) as originally planned.

The scaling up activities included:

- Civil works to allow for upgraded ventilation of the BR as well as for the installation of the boiler's chimney towards the building's exterior.
- Piping installation for connection with the HRS and for water drainage towards the building's exterior
- H_2 grid modifications with upgraded pressure regulators and relief valves as well as new piping for the supply of H_2 to the burner and for venting

Figure 3. Prototype H_2 burner and condensing boiler.

2.3 H_2 compressor

The H_2 compressor (Figure 4) was supplied by CRES, while NTUA undertook the maintenance and testing procedures necessary to verify the operational state of the compressor as well as the supervision of the integration activities.

Figure 4. H_2 compressor.

The installation of the compressor was carried out in four stages: firstly, the compressor was partially disassembled and all safety release valves were tested and verified for proper operation. Then, in order to ensure the adequate cooling of the compressor, a closed hydraulic circuit using a water chiller was installed. The compressor was then connected to the H_2 distribution grid and finally the EMCS was programmed so as to enable the automatic operation of the compressor.

The applied logic dictates that when the pressure inside the buffer storage cylinders (i.e. the compressor's inlet pressure) becomes higher than a user defined value (current setpoint is 6 bar), the compressor starts. A pressure switch automatically stops the compressor when the inlet pressure falls below 1.8 bar.

2.4 Pressure cylinder stacks

Concerning the pressure cylinder stacks, three more stacks were provided from VÍTKOVICE CYLINDERS (Figure 5). Each cylinder stack contains twelve 80 lt (water capacity) pressure cylinders. Their connection to the H_2 distribution grid was made using stainless steel flexible pipes and was easily accomplished since appropriate tapped connecting valves were foreseen during the small-scale phase. With the

integration of the additional cylinder stacks, the total water volume of the storage is currently 3480 lt. Under a pressure of 200 bar, this water volume corresponds to approximately 690 Nm^3 or 61 kgr of gaseous H_2.

Figure 5. New pressure cylinder stacks for the storage area.

It should also be noted that extensive upgrades and modifications were also performed to the electrical installation of the demonstration building as well as the GenConStore area in order to meet the specifications and requirements of the large-scale equipment.

3. GENERAL OVERVIEW AND TECHNICAL DESCRIPTION OF THE FULL SCALE PROTOTYPE

The full-scale prototype plant aimed at assessing the efficiency and performance of the entire system and its components under real conditions. Furthermore, the safety and techno-economic evaluation of the developed energy system would also be investigated during this phase of the project. Section 3 of this report provides a detailed description of the full-scale prototype, while the performance and efficiency analysis of each individual component as well as the entire RES-H_2 system is carried out in Section 4. The techno-economic evaluation is presented in deliverable D11.1.

3.1 RES-H_2 hybrid energy system

The full-scale RES-H_2 hybrid energy system consists of the Renewable Energy Sources (RES), the H_2 production, storage and consumption equipment as well as the systems responsible for monitoring, management and safety of operation. In detail, these components are:

- RES, namely photovoltaic (PV) panels (total installed power 46.8 kW) and wind turbines (total installed power 36 kW) to harvest primary (solar and wind) energy.
- Water electrolysis (EL) unit (22.3 kW) to produce gaseous H_2.
- H_2 distribution grid and H_2 storage vessels (max water capacity 3480 lt).
- H_2 compressor to enable the gaseous H_2 storage in high pressure (up to 200 bar).
- Micro-CHP fuel cell (FC) (20 kWel and 20 kWth) with peripherals (air blower, water deionization system, control cabinet, DC to AC inverter etc.) to convert the stored H_2 to electrical and thermal energy.
- Prototype H_2 burner with a condensing boiler (60 kWth) to convert the stored H_2 to thermal energy.
- Heat Recovery System (HRS) to exploit the thermal energy produced by the FC and the H_2 burner.
- Energy Management and Control System (EMCS), which is described in detail in Deliverable D7.3, to control the flow of energy by managing RES and control devices, to monitor system operation, to maximize efficiency and to ensure reliability in system operation.
- Safety and Protection System (SPS), to guarantee the safety of the full-scale installation and the occupants of the building.

All of the above systems, except the RES and the EMCS, are installed in a specially designed and constructed area of the demonstration building that is called GenConStore area, since it hosts the equipment for the generation, consumption and storage of H_2.

3.1.1 Heat Recovery System (HRS)

The HRS was designed in order to increase the overall efficiency of the RES-H_2 system by recovering the thermal energy produced by the FC and the H_2 burner. The thermal energy produced by the micro-CHP and the H_2 Burner is stored in the form of hot water in a large tank (called “puffer” tank). According to demand, this water can be used to cool the micro-CHP or it can be circulated, using appropriate piping and pumps, through a plate heat exchanger towards the demonstration building’s HVAC unit when heating is needed in order to save on electric energy consumption.

The P&ID of the HRS is given in Figure 6, while photographs of various HRS components can be seen in Figures 7 and 8.

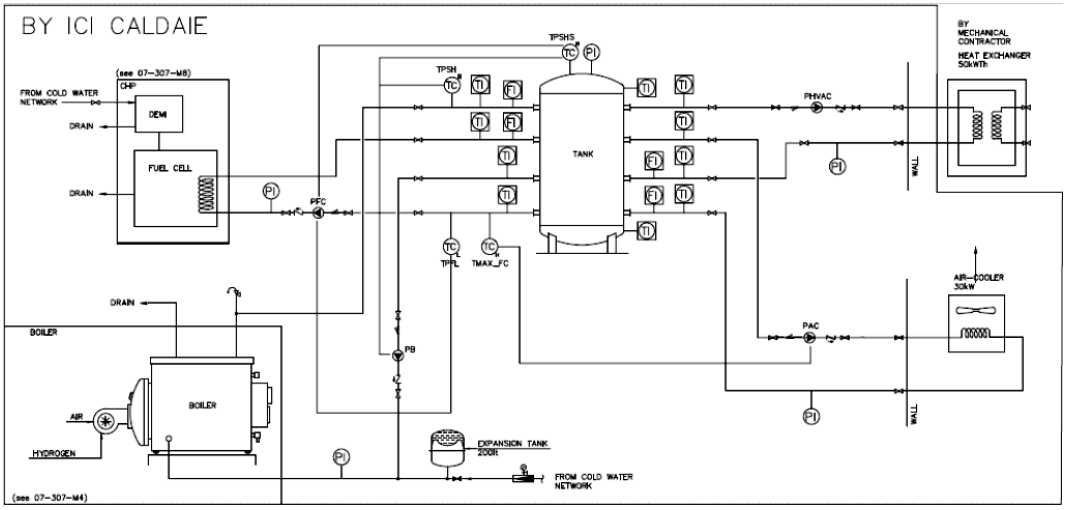

Figure 6. P&ID of the HRS.

Figures 7 (left) and 8 (right). HRS “puffer” tank and plate heat exchanger connected to HVAC unit respectively.

3.1.2 Energy Management and Control System (EMCS)

The EMCS consists of two sub-systems, the monitoring system and the control system. The monitoring sub-system is using smart metering devices to measure and store the values of selected parameters based on the Modbus protocol. The measurements are fed to the control sub-system that incorporates the full-scale plant control algorithm according to which the operation of equipment and flow of energy are managed. The architecture of each sub-system is shown in Figures 9 and 10 respectively.

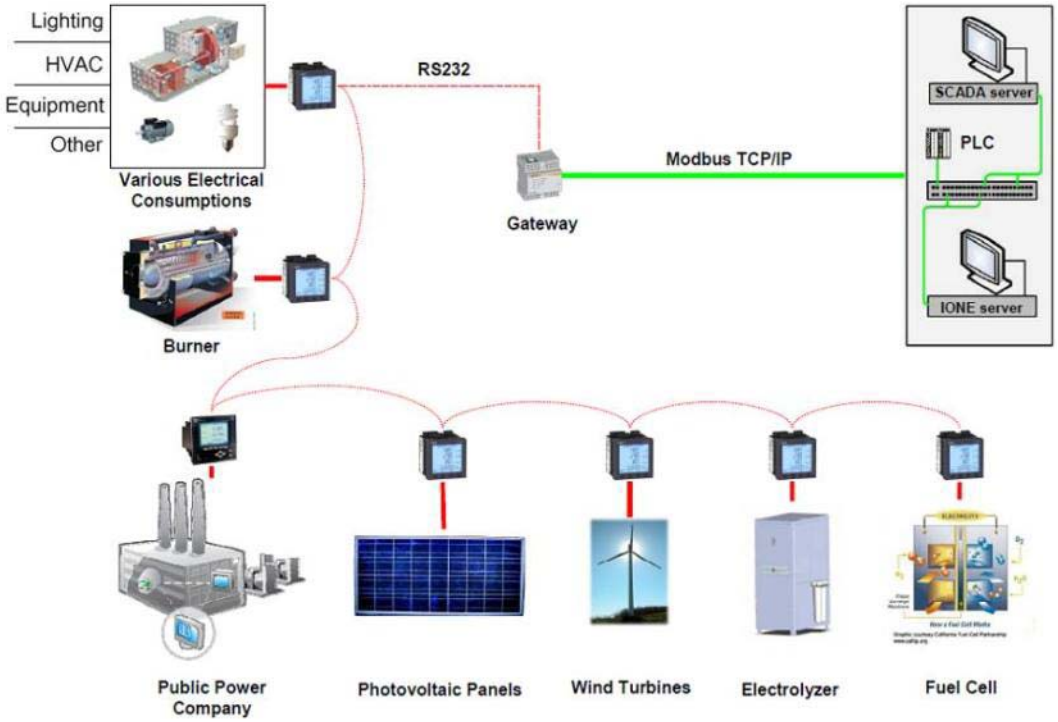

Figure 9. Architecture of the monitoring sub-system of the EMCS.

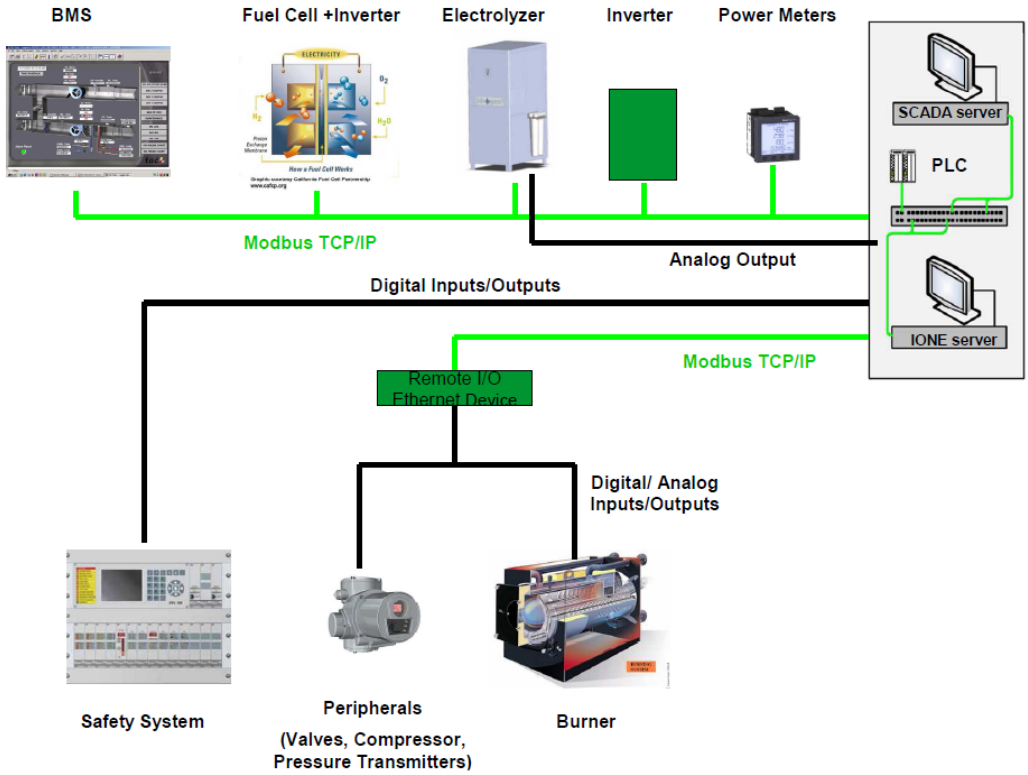

Figure 10. Architecture of the control sub-system of the EMCS.

For an extensive analysis of the EMCS, deliverable D7.3 should be used as reference.

The implemented logic of the RES-H_2 system operation is based on the balance between the produced energy and the consumed energy. The energy harvested from the RES is directly used to cover the building's contingent loads. In case of excess energy, this is converted to gaseous H_2, by means of the EL, to be used as energy storage material. In case of energy shortage, the stored H_2 is applied as a green fuel to cover the electrical and thermal needs of the building by means of the FC and the H_2 burner.

The calculation of the difference between the total energy that is being produced by the full-scale prototype plant minus the total energy that is being consumed is performed in 5 min intervals and depending on this value, appropriate commands are issued. The primary goal of the control algorithm is to achieve a Zero Energy Building (ZEB), thus resulting in zero energy exchange with the public power grid and zero CO_2 emissions.

The plant operator(s) can interact with the EMCS through the developed GUI that provides a unified interface for, almost real-time, system operational status monitoring and control. This GUI is based on the full-scale plant's mimic diagram (Figure 11) and its full functionality is described in the final section of this report (Operation manual).

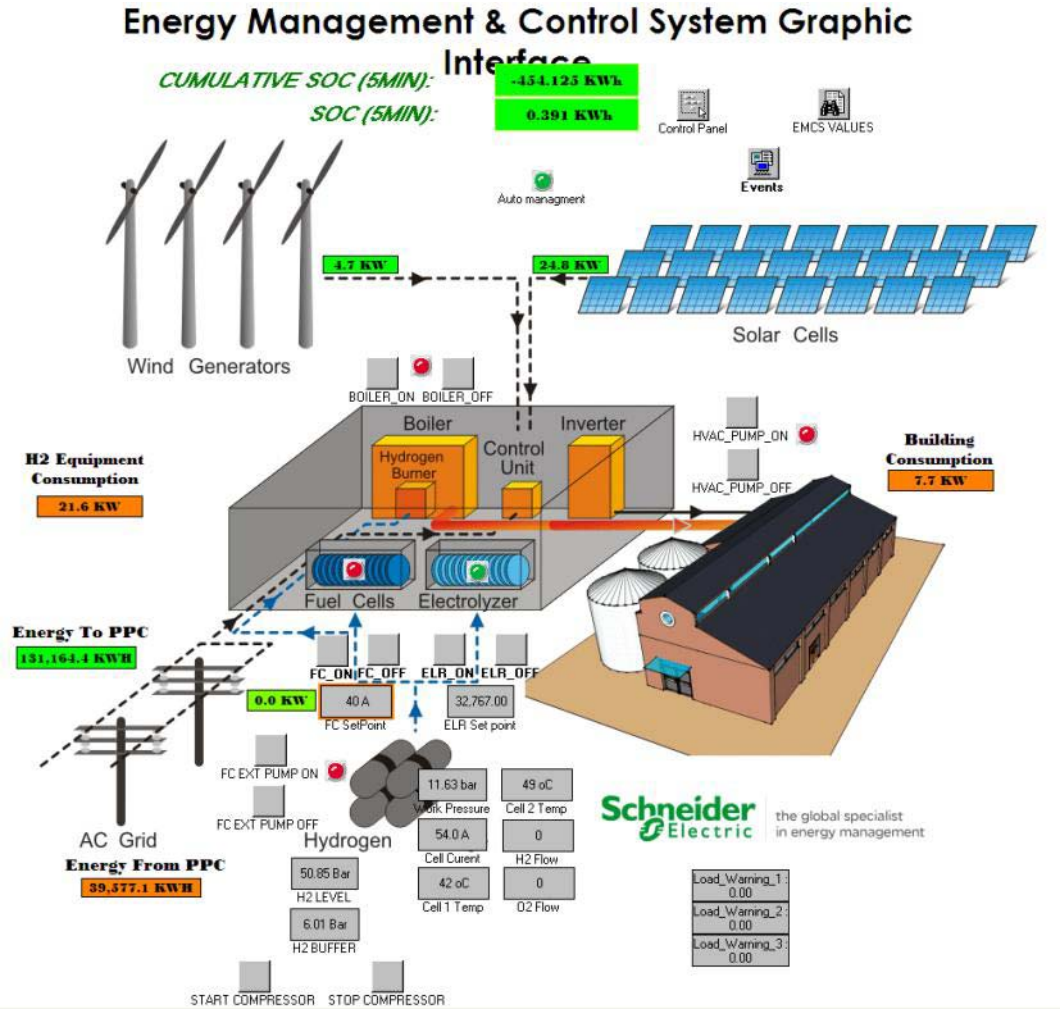

Figure 11. Developed GUI for the EMCS.

3.1.3 Safety and Protection System (SPS)

The SPS manages signals that are collected from different types of detectors and integrates safety measures and procedures that are initiated in case of alarm. The detectors have been mainly installed in the GenConStore area and their exact placement is shown in Figure 12.

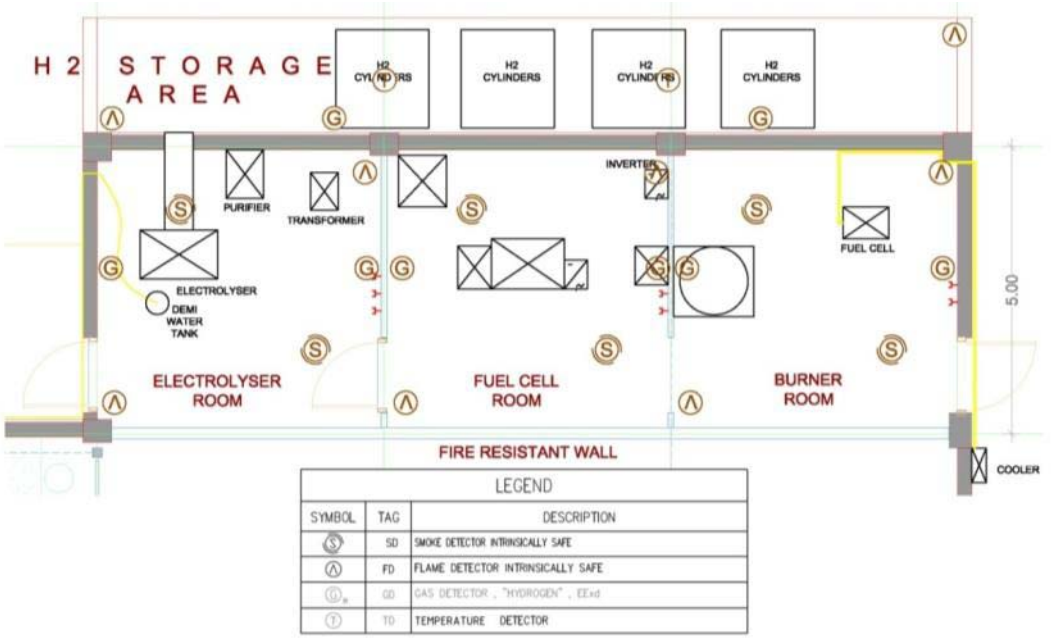

Figure 12. SPS detector placement in the GenConStore area.

Specifically, the following detectors have been installed:

- H_2 detectors to check for increased H_2 levels, indicating H_2 leakage
- Infrared flame detectors to check for fire fuelled by H_2, since this kind of fire can only be detected by the produced heat
- Smoke detectors to check for fire caused by other sources
- Contact switches on the H_2 GenConsStore area entrances
- Local control panels next to the H_2 GenConsStore area entrances
- Electromagnetic valves in different sections of the H_2 distribution grid
- Heat sensors to monitor ambient temperature
- An inert gas (N_2) extinguishing system that floods the H_2 GenConsStore area in case of a severe alarm
- Audiovisual alarms

For the rest of the building space, standard smoke and motion detectors have been also installed for safety and security reasons.

In case that an alarm occurs, the SPS will inform predefined recipients and depending on the type of alarm a series of pre-configured procedures will be activated. These procedures include (but are not limited to) the isolation of the H_2 distribution grid and storage cylinders using the electromagnetic valves, the

termination of equipment operation, the activation of the fire extinguishing system etc.

All signals and procedures can be managed through the SPS cabinet that is installed inside the plant's Control Room (Figure 13). The functionality of the SPS is described in the final section of this report (Operation manual).

Figure 13. SPS cabinet.

3.2 Demonstration building

3.2.1 Building description

The demonstration building is located inside the Lavrion Technological and Cultural Park (LTCP), which is located in the city of Lavrion, in the South-Eastern Attica region, approximately 50 km from Athens, Greece.

The building envelope consists of a concrete structure with double brick walls and non-insulated single-glazed windows. The roof consists of metallic panels with 1" polyurethane insulation layer in the middle. The overall dimensions of the selected building are 30.50 m x 15.50 m, with a maximum height of approximately 8.35 m. The building has a ground floor with a surface area of approximately 375 m^2 and an attic floor with an area of approximately 150 m^2 (total surface area approximately 525 m^2). The ground floor hosts a waiting area, a small kitchen, WCs, the control room and the main area (Figure 14). The attic also hosts a waiting area, two offices and a meeting room (Figure 15).

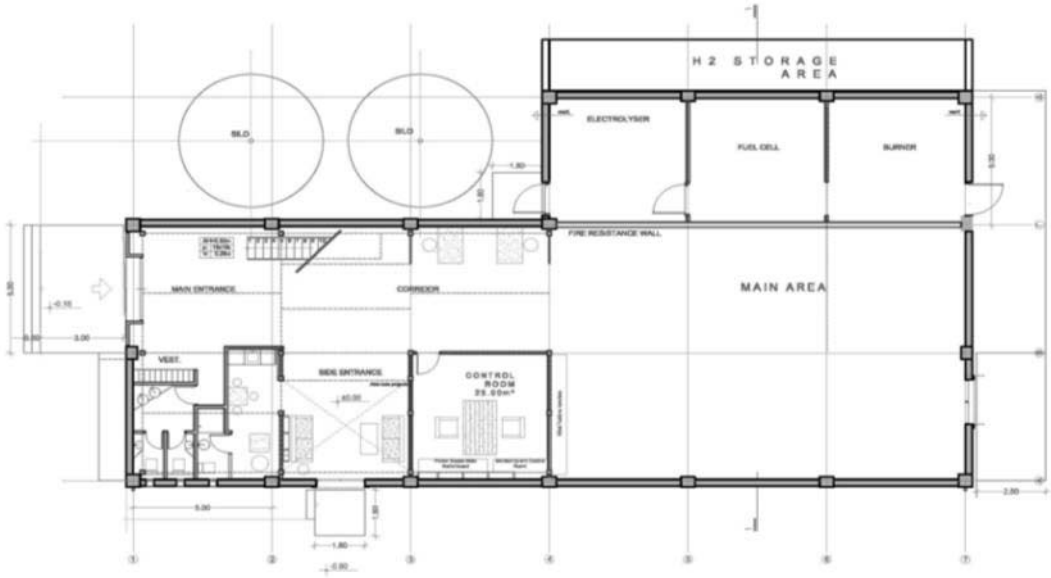

Figure 14. Down view of ground floor in the demonstration building.

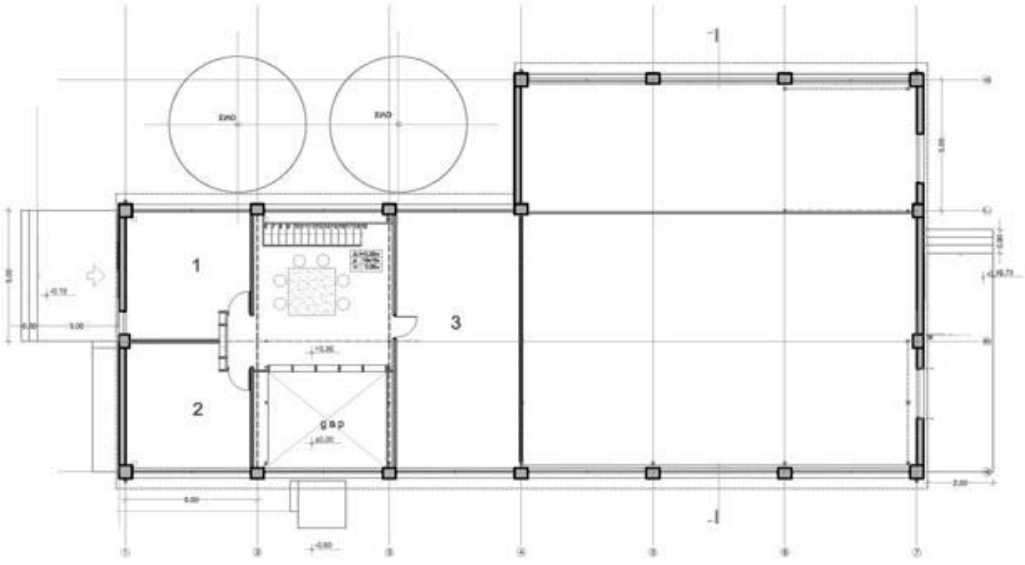

Figure 15. Down view of attic in the demonstration building.

Figures 16 and 17 provide a 3D interior and an exterior view of the demonstration building respectively.

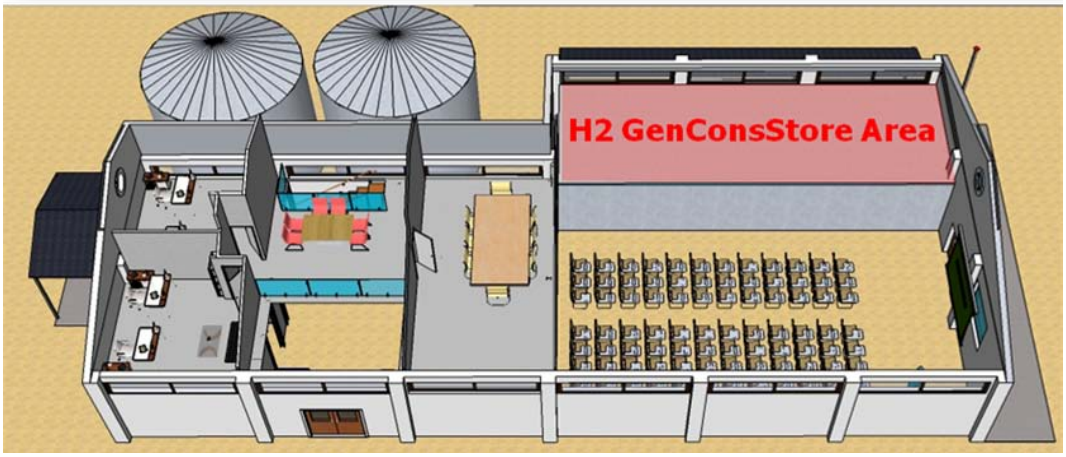

Figure 16. 3D aspect of building's interior.

Figure 17. Demonstration building external aspect.

3.2.2 Building loads

The building loads are grouped as follows:

- Lighting: for the interior lighting of the building, a total of 48 lighting fixtures, each with 2x36 W fluorescent bulbs are used, resulting in a total load of approximately 3.5 kW. Four halogen headlights, each consuming approximately 250 W, are also used to illuminate the exterior of the building during the night.
- HVAC: two separate systems are used to cover the heating/cooling and ventilation needs of the building. The first is based on exterior VRV units (Figure 18) and floor mounted fan-coils (maximum electrical load is approximately 25 kW).

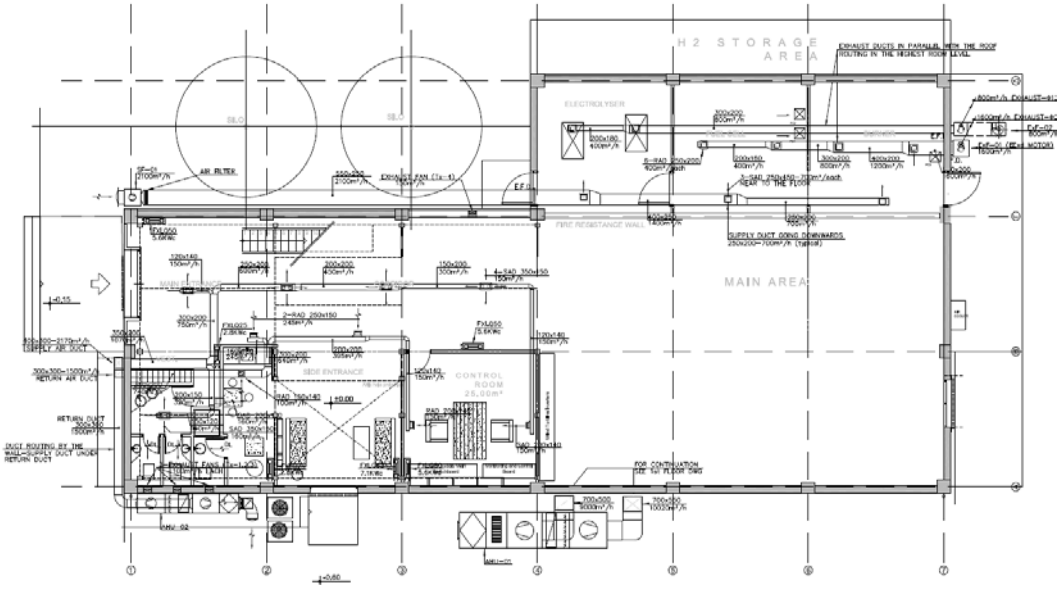

Figure 18. VRV system layout (heat pump is also shown on the bottom middle).

The second is a combination of a heat pump with an AHU (Figure 19), able to use the hot water from the HRS in order to decrease its electrical energy consumption when the building needs to be heated (maximum electrical load without taking into consideration the HRS is approximately 32 kW).

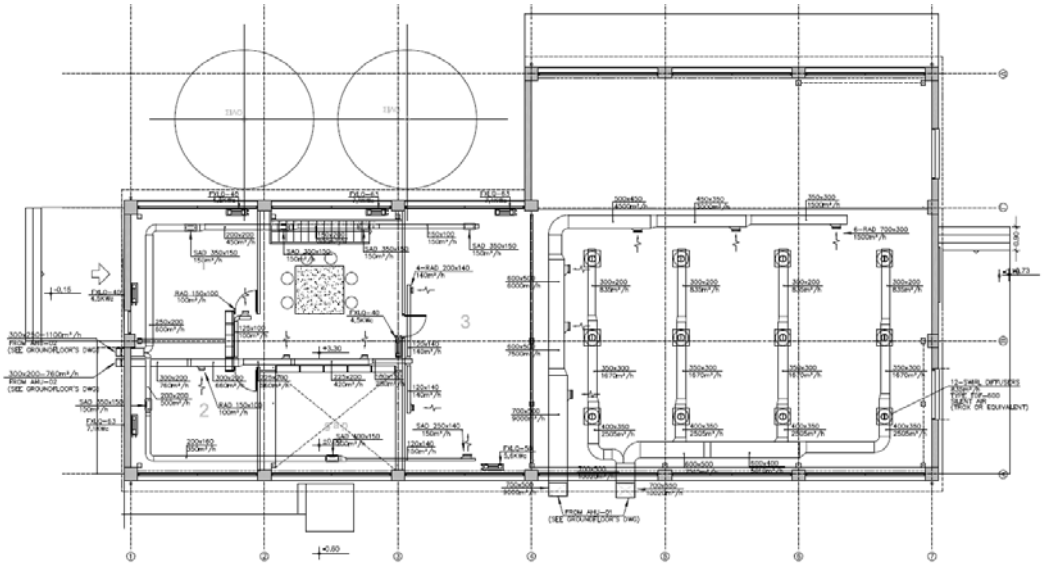

Figure 19. Airduct layout for the heating, cooling and ventilation of the building.

- Offices, meeting room and main area consumptions involve two desktop PCs, one laser printer/scanner/copier/fax machine, and other general office equipment. For specific cases (large meetings, team presentations etc.), two laptop computers and a projector are also used. Maximum electrical load is estimated around 3 kW and varies with occupancy.

The detailed technical specifications of building loads are presented in the appropriate section discussing the performance evaluation of the full-scale demonstration building.

4. PERFORMANCE EVALUATION

The performance evaluation of the full-scale prototype plant was based on data collected by the monitoring sub-system of the EMCS under real operating conditions. More specifically, from the group of all recorded magnitudes, the analyses were mostly based on the energy and power measurements. As far as energy is concerned the recorded measurement that was used corresponds to the cumulative value since the monitoring system installation. All measurements are recorded in 1 min intervals.

The evaluation concerns the whole of 2011 and the most recent period between February and September of 2012. January of 2012 is not included in the analysis because there were frequent stops to allow for programming modifications, upgrades and maintenance activities to the system.

A common presentation format is used for the performance evaluation results of each component. Initially, the component's description and technical specifications are given, followed by a short description of the appropriate performance parameters, calculations and results. Subsequently, maintenance issues (if occurred) or other general issues encountered during operation are also reported. Finally, the lessons learned and conclusions drawn are discussed.

4.1 RES

The data for the performance evaluation of the RES refer to the entire 2011 in order to account for seasonal variations. The evaluation is carried out separately for the photovoltaic (PV) and wind turbine (WT) systems. The same evaluation is also carried out for the most recent period (i.e. between February 2012 and September 2012). Before presenting the RES performance evaluation, a description of the local meteorological data is given based on the measurements from a Davis Vantage Pro2 Plus weather station that is installed in the same area as the demonstration plant.

4.1.1 Meteorological data

4.1.1.1 Description

The meteorological conditions in the area of the full-scale prototype plant are monitored using a Davis Vantage Pro2 Plus weather station, located on the same hill that the WTs are installed. This weather station includes two components: the Integrated Sensor Suite (ISS), which houses and manages the external sensor array, and the console, which provides the user interface, data display, and calculations.

4.1.1.2 Measured parameters

The measured meteorological conditions include (among others) barometric pressure, dewpoint calculation, heat index, relative humidity, temperature, solar radiation, UV radiation, wind speed and wind direction, rain rate, rain fall etc. The above parameters are recorded every 15 minutes and all measurements are transmitted wirelessly to the demonstration building and are stored in a SQL database.

Tables 1 and 2 list the most important meteorological data that were used in the performance analyses of the RES. These parameters include the solar radiation and ambient temperature for the PVs and the wind speed for the WTs. Precipitation measurements are also included. Table 1 refers to the data collected throughout 2011 and Table 2 refers to the data for the period February 2012 – September 2012.

Table 1. Average values of meteorological data during 2011.

Month	Average Solar Radiation (kWh/m^2)	Average Temperature (^{o}C)	Average Wind Speed (m/sec)	Precipitation (mm)
January	2.942	10.45	1.991	75.4
February	3.444	10.70	2.964	182.8
March	4.386	11.33	2.949	39.6
April	5.627	13.99	3.547	63.2
May	6.512	18.74	2.188	8.8
June	6.796	24.26	1.816	1.6
July	8.373	28.39	2.165	0.0
August	6.212	27.19	4.163	0.0
September	6.457	25.17	3.537	18.6
October	4.861	17.05	3.744	29.2
November	3.478	12.38	3.953	0.8
December	3.234	11.70	0.689	36.6

Table 2. Average values of meteorological data from February 2012 until September 2012.

Month	Average Solar Radiation (kWh/m^2)	Average Temperature (^{o}C)	Average Wind Speed (m/sec)	Precipitation (mm)
February	3.106	9.67	2.250	54.8
March	5.339	12.50	2.361	12.2
April	6.265	17.00	1.917	23.2
May	6.735	20.83	1.778	7.4
June	7.677	26.79	3.059	0.0
July	7.403	29.45	2.603	0.0
August	6.981	29.92	2.676	0.0
September	5.828	24.89	2.224	0.0

The variations of the solar radiation, temperature and wind speed for all periods are presented in Figures 20 - 22.

As is evident from the above, during the period of February 2012 until September 2012, average solar radiation was higher compared to the corresponding period of 2011, therefore energy production from PV panels is expected to be higher for this

period. However, average temperatures during 2012 were also higher so this may impact the performance ratio unfavourably.

At the same time, average wind speed was lower compared to the corresponding period of 2011, therefore energy production from WTs is expected to be lower.

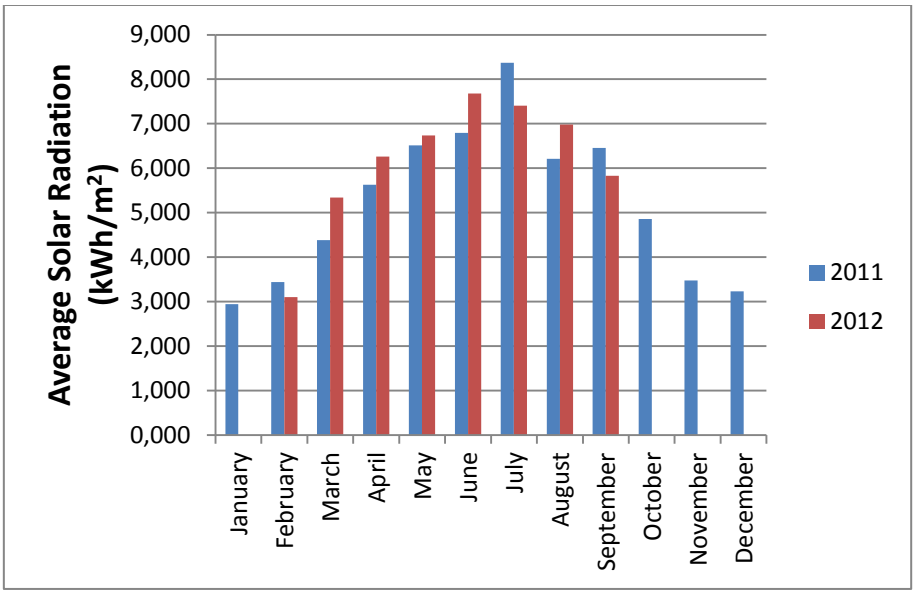

Figure 20. Variation of average solar radiation per month.

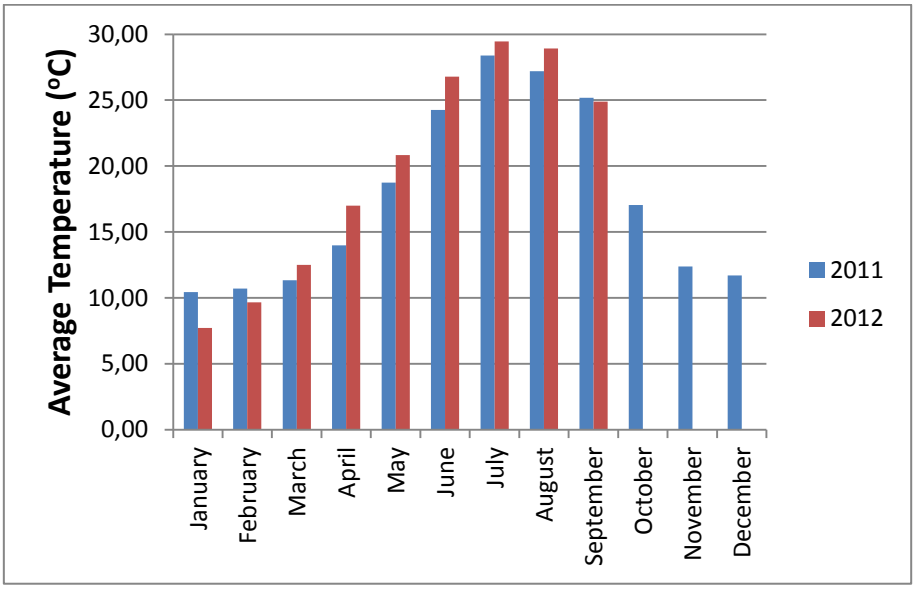

Figure 21. Variation of average temperature per month.

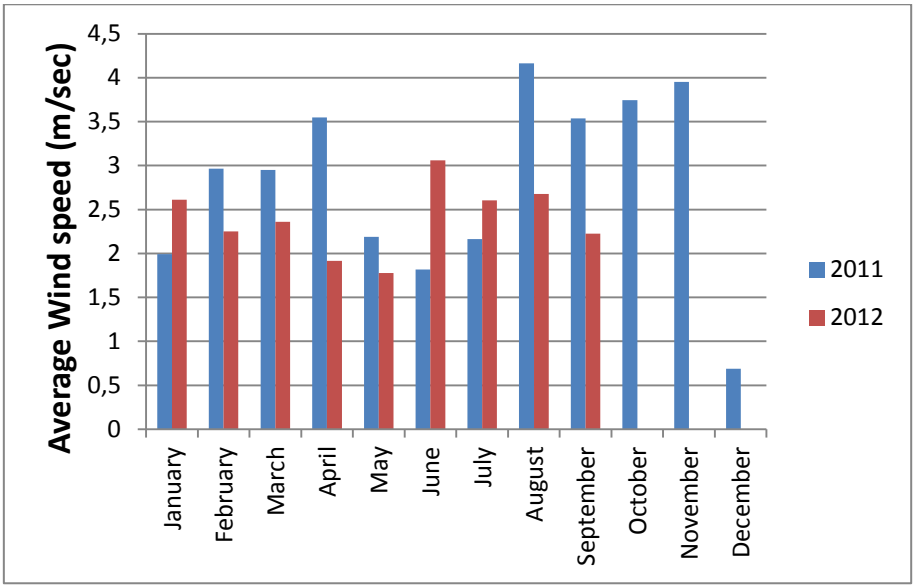

Figure 22. Variation of average wind speed per month.

4.1.1.3 Conclusions

The installed weather station allows for continuous measurement and recording of the meteorological conditions in the demonstration site area. The recorded data are necessary to conduct simulations of the expected energy production from the RES as well as for the calculations involved in the RES performance evaluation.

In this regard, the wireless data transmission and the remote management capabilities of the weather station are very important features that offer enhanced functionalities, which enable the automation of the above procedures (for example data synchronization, energy production forecasting etc).

4.1.2 PV system

4.1.2.1 Technical specifications

The installed PV panels are based on thin film CIGS technology (Table 3). A total of 624 panels have been installed in the roof of a nearby building facing directly South and at an inclination of approximately 23 degs. Total panel area is 474.65 m^2 and total installed power is 46.8 kW.

The produced DC current is transformed to AC through six SMA Sunny Mini Central 8000TL inverters (Table 4). The inverters feature power balancing characteristics and are connected in pairs to form a 3-phase supply to the demonstration building. It should be noted that although each inverter is connected to 104 PV panels, these are not symmetrically distributed on the roof (due to the fact that the latter is constructed in three different levels) resulting in differences in the produced energy among the inverters.

Table 3. Specifications of PV panels.

Product Name			SL1-75F
Nominal Efficiency	n	%	9.8
Nominal Power (+5/-0 W)	P_{max}	W	75.0
Short Circuit Current	I_{OC}	A	1.58
Open Circuit Voltage	V_{OC}	V	72.3
Current at Maximum Power	I_{mp}	A	1.37
Voltage at Maximum Power	V_{mp}	V	56.9
Dimensions	W x H x D	m	0.636 x 1.196 x 0.036

Table 4. Specifications of DC/AC inverters.

Product Name		SMC 8000TL
Max DC Power	W	8250
Max DC Voltage	V	700
Max Input Current	A	25
Max AC Power	W	8000
Max Output Current	A	35
AC Voltage Range	V	180 – 260
AC Frequency	Hz	50
Max Efficiency	%	98

4.1.2.2 Measured parameters and calculations

There are three performance parameters that are used to define the overall system performance with respect to energy production, solar resource and overall effect of system losses for PV systems. These parameters are the final PV system yield, reference yield and performance ratio.

The final PV system yield (Y_f) is the net energy output E divided by the nameplate DC power P_o of the installed PV array (Equation 1).

— (Equation 1)

The reference yield (Y_r) is the total in-plane irradiance H divided by the PV's reference irradiance G (in the case of the project's installed PV panels, G refers to the Standard Test Conditions and is equal to 1000 W/m^2) (Equation 2).

– (Equation 2)

The performance ratio (PR) is the Y_f divided by the Y_r (Equation 3). Since PR normalizes with respect to irradiance, it quantifies the overall effect of losses due to inverters and wiring, PV panel temperature, soiling or snow, system downtime and component failure. PR values normally fall within the range of 60 – 80% (Marion et al., 2005).

— (Equation 3)

The monthly analysis of 2011 is shown in Tables 5 and 6. Table 5 shows the energy produced per inverter as well as the energy that is finally delivered to the building. Table 6 shows the difference in energy produced and energy delivered to building, the three performance parameters (Y_f, Y_r, PR) as well as the peak power output for each month.

Table 5. Energy produced by PV system for 2011.

Month	Energy produced - Inverter 1 (kWh)	Energy produced - Inverter 2 (kWh)	Energy produced - Inverter 3 (kWh)	Energy produced - Inverter 4 (kWh)	Energy produced - Inverter 5 (kWh)	Energy produced - Inverter 6 (kWh)	Energy delivered to Building (kWh)
January	623.680	613.490	658.500	531.310	580.860	610.400	3074.284
February	608.420	637.680	677.210	561.230	566.740	592.420	3761.744
March	906.480	894.450	950.950	782.750	849.750	877.580	5267.133
April	1124.820	1114.600	1180.800	967.940	1051.330	1089.810	6519.582
May	1330.440	1324.110	1397.520	1141.260	1242.700	1288.080	7712.436
June	1328.190	1327.810	1400.240	1129.720	1235.640	1302.310	7700.301
July	1407.650	1415.980	1495.230	1188.830	1306.290	1390.620	8165.225
August	1315.770	1331.800	1420.140	1099.790	1201.370	1322.890	7652.856
September	1136.440	1154.280	1242.530	938.050	1026.020	1162.910	6623.159
October	888.750	902.870	984.230	723.530	794.420	909.490	5190.079
November	589.650	600.170	666.410	473.220	515.910	614.650	3463.851
December	571.820	583.290	646.870	453.730	502.780	596.300	3361.690
TOTAL	**11832.110**	**11900.530**	**12720.630**	**9991.360**	**10873.810**	**11757.460**	**68492.340**

Table 6. Performance evaluation of PV system for 2011.

Month	Difference (kWh)	Difference (%)	System yield Yf (kWh/kW)	Reference Yield Yr	Performance ratio (%)	Peak Power (kW)
January	543.956	15.034	65.690	91.215	72.016	46.000
February	-118.044	-3.240	80.379	96.439	83.347	48.000
March	-5.173	-0.098	112.546	135.967	82.774	47.900
April	9.718	0.149	139.307	168.811	82.523	47.900
May	11.674	0.151	164.796	201.868	81.635	47.880
June	23.609	0.306	164.536	203.868	80.707	47.810
July	39.375	0.480	174.471	259.578	67.213	38.480
August	38.904	0.506	163.523	192.573	84.915	41.050
September	37.071	0.557	141.520	193.696	73.063	41.470
October	13.211	0.254	110.899	150.698	73.590	47.750
November	-3.841	-0.111	74.014	104.338	70.937	40.900
December	-6.900	-0.206	71.831	100.247	71.654	40.120
TOTAL	**583.560**	**0.845**	**1463.512**	**1899.298**	**77.055**	

As can be seen from the Tables above, the difference between the energy production as reported by the inverters and as reported by the monitoring system is approximately 0.845% thus no unexpected losses are observed in the energy transfer from the PV installation to the building.

Figure 23 illustrates the measurements of Table 5. The differences in the produced energy per inverter were expected, since as already mentioned, the PV panels are not symmetrically installed on the different levels of the roof causing variations in local shading effects and wind exposure that can influence panel temperature. Of course, the produced energy is higher during summer with the highest values recorded in July.

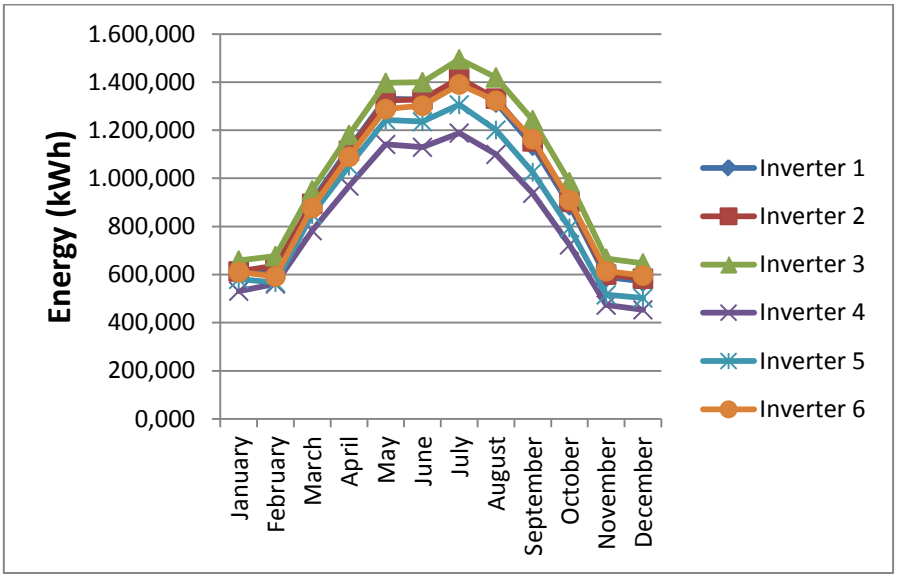

Figure 23. Energy produced per inverter of the PV system for 2011.

The yearly Y_f is 1463.512 Kwh/kW, which is above average for the area of Attica in Greece (approximately 1300 – 1400 kWh/kW (PVGIS, 2001-2007)). Total energy production during 2011 was 68492.340 kWh.

Figure 24 presents the PR variance per month. As can be seen, PR values range from 67% to 85%, with only one month below 70%, which again can be characterized as very good (Goetzberger et al., 2005).

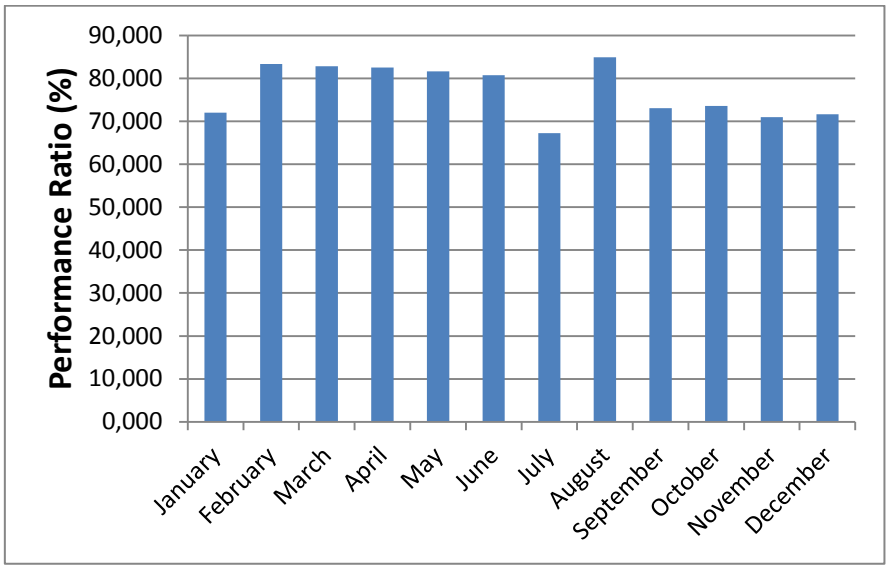

Figure 24. PR values of PV system for 2011.

Similarly, Tables 7 and 8 present the same data for the period February to September 2012 as this is the most recent period.

Table 7. Energy produced by PV system from February to September 2012.

Month	Energy produced - Inverter 1 (kWh)	Energy produced - Inverter 2 (kWh)	Energy produced - Inverter 3 (kWh)	Energy produced - Inverter 4 (kWh)	Energy produced - Inverter 5 (kWh)	Energy produced - Inverter 6 (kWh)	Energy delivered to building (kWh)
February	488.260	498.230	554.350	385.300	424.120	506.360	2866.470
March	947.910	967.780	1056.020	773.830	849.570	967.690	5544.810
April	1059.040	1080.420	1178.440	857.770	945.320	1078.470	6177.320
May	1138.400	1160.220	1265.920	911.610	1006.400	1158.640	6612.060
June	1232.880	1254.550	1369.280	982.480	1084.110	1243.560	7129.970
July	1164.740	1180.620	1304.150	900.710	1005.240	1194.860	5906.660
August	1057.060	1068.640	1199.030	786.000	884.130	1101.850	5675.450
September	849.720	858.970	981.270	602.690	687.690	893.360	4860.270
TOTAL	**7938.010**	**8069.430**	**8908.460**	**6200.390**	**6886.580**	**8144.790**	**44773.010**

Table 8. Performance evaluation of PV system from February to September 2012.

Month	Difference (kWh)	Difference (%)	System yield Yf (kWh/kW)	Reference Yield Yr	Performance ratio (%)	Peak Power (kW)
February	-9.850	-0.345	61.249	90.077	67.997	46.900
March	17.990	0.323	118.479	165.514	71.582	45.210
April	22.140	0.357	131.994	187.954	70.227	47.310
May	29.130	0.439	141.283	208.771	67.674	47.440
June	36.890	0.515	152.350	230.301	66.152	42.250
July	843.660	12.498	126.211	229.504	54.993	33.700
August	421.260	6.910	121.270	216.397	56.041	35.780
September	13.430	0.276	103.852	174.825	59.403	37.140
TOTAL	**1374.650**	**2.979**	**956.688**	**1503.343**	**63.637**	

Figure 25 illustrates the measurements of Table 7. The graphs follow the same pattern as the yearly results (gradually increasing energy production from February until June), however the actual energy produced is slightly lower for all months except March compared to the same period in 2011.

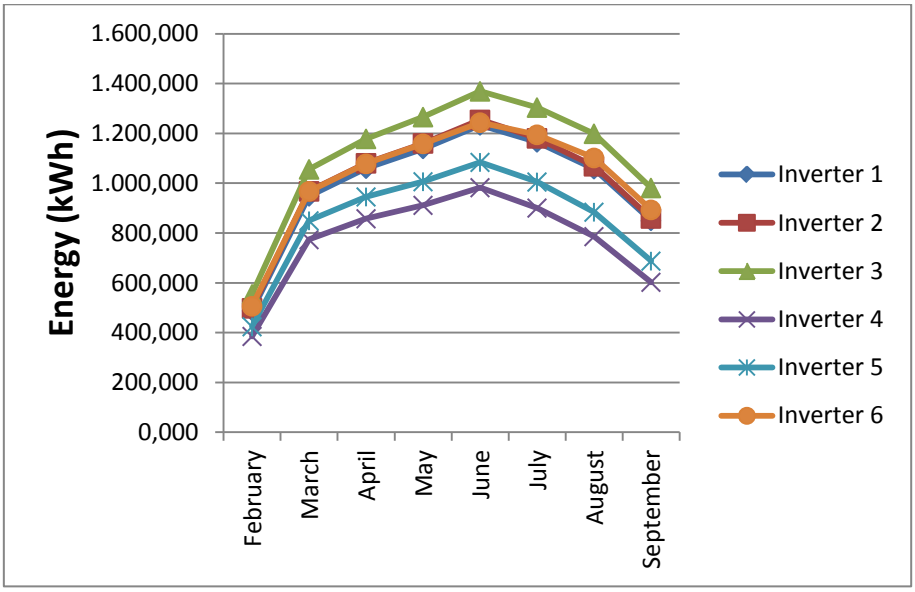

Figure 25. Energy produced per inverter of the PV system from February to September 2012.

By examining the PR values (ranging from approximately 55% to 72%, Figure 26), a decrease in performance compared to the same period in 2011 is also observed. Despite this fact, the overall PR of the period is 63.64%, resulting in efficient operation of the PV system.

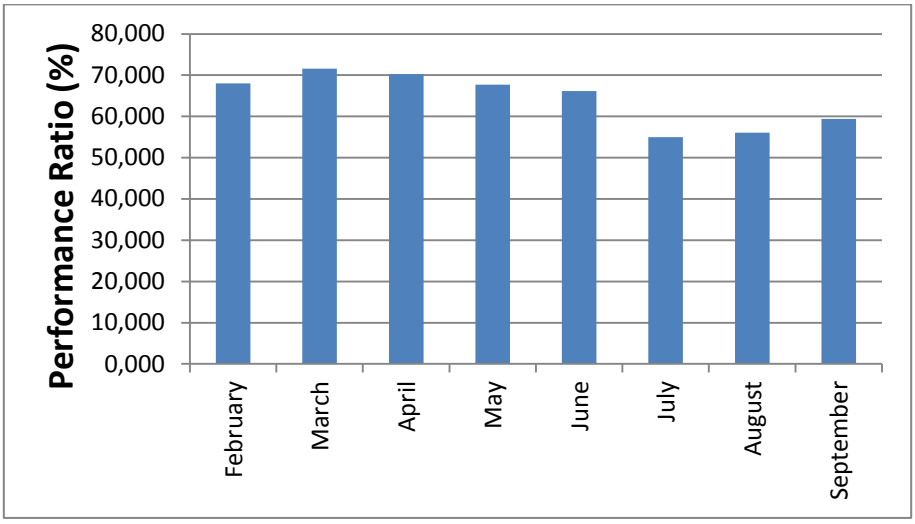

Figure 26. PR values of PV system from February to May 2012.

Comparing the Y_r of the two periods (2011 and 2012), it is shown that the behavior of the PV system is not consistent. The energy production variation between the two periods matches the Y_r variation between the two periods only for February, March, July and September. At the same time, the opposite behavior is presented for April, May, June and August.

Taking the PR into consideration, it is also clear that there is an overall decrease for 2012. Since the average temperature differences are not high enough to account for such an effect to PR and since it is not possible for the PV panels to exhibit an approximate 15% PR reduction in one year, the most probable explanation is soiling

(dust accumulation) on the PV panels. This is verified after examining the rain data for these periods. As can be seen from Tables 1 and 2, there is a distinctive decrease in precipitation during 2012 compared to 2011. Since there is no other implemented method of cleaning the PV panels except rainfall, the result is increased soiling and decreased energy production.

4.1.2.3 Maintenance and/or failures

Based on the measured energy production and PR decrease, a maintenance activity involving the cleaning of the PV panels was performed to address the soiling problem. Furthermore, a periodic cleaning plan will be put in effect, especially after long periods without rain or with strong winds, to avoid the re-appearance of this problem.

No failures have been observed since the installation of the PV system. The only problem encountered was the loss of internet connectivity on a couple occasions, for which the ISP was responsible, resulting in minor loss of data for the respective periods.

4.1.2.4 Conclusions

Given the calculated Y_f and PR values, the PV system has performed very well during 2011. The increased performance can be attributed mainly to the fact that the PV panels are based on thin film CIGS technology that exhibits better behavior under low-light or shading conditions and increased temperatures in comparison to other PV module technologies (Powalla et al., 2004).

The most recent data of 2012 show a decrease in performance compared to 2011, the main reason for which is soiling on the panels. A periodic maintenance including cleaning of the panels was planned to deal with this problem and increase overall energy production.

4.1.3 WT system

4.1.3.1 Technical specifications

The WT system consists of six wind turbines that are installed in a hill approximately 50 m from the demonstration building. The selected wind turbines are based on downwind technology and are equipped with a flexible blade system connected to a permanent magnet generator that enables the wind turbine to generate power in light as well as in strong winds. The blades are held by springs that allow them to pitch and cone in high wind speeds in order to reduce the induced stresses. The turbine frame also includes a service brake that acts on the rotor shaft and is used for maintenance purposes.

The mast that is connected to the turbine frame has a steel base plate that incorporates a raising and lowering mechanism. The top of the mast has a yaw bearing assembly that permits the rotation of the turbine frame enabling the rotor to turn 360^0 and self orientate depending on wind direction and speed.

The technical specifications of the WTs are shown in Table 9.

Table 9. Specifications of installed WTs.

Product Name		Proven 6
Max Power	**kW**	6
Cut-in Speed	**m/sec**	2.5
Rated Speed	**m/sec**	12
Rotor Type		Downwind, Self regulating
No of Blades		3
Blade Diameter	**m**	5.5
Rated RPM	**RPM**	200
Hub Height	**m**	9

4.1.3.2 Measured parameters and calculations

The performance evaluation focused on examining the effect of each WT placement on its energy production, the WT system yield (energy produced per installed kW) as well as the correlation between energy production and average wind speeds.

The monthly analysis of 2011 is shown in Tables 10 and 11. Table 10 shows the energy produced per inverter (i.e. per WT) and the total energy that is delivered to the building. Table 11 shows the differences between the produced energy and the energy delivered to the building, the system yield and the peak power output.

It must be noted that due to the fact that the data logger for each WT was installed in middle of March 2011, the measurements per inverter fom the start of the year until that date are unavailable and therefore this period is not included in the year total calculations.

Table 10. Energy produced by WT system for 2011.

Month	Energy produced - Inverter 1 (kWh)	Energy produced - Inverter 2 (kWh)	Energy produced - Inverter 3 (kWh)	Energy produced - Inverter 4 (kWh)	Energy produced - Inverter 5 (kWh)	Energy produced - Inverter 6 (kWh)	Energy delivered to building (kWh)
January	-	-	-	-	-	-	2120.598
February	-	-	-	-	-	-	3597.191
March	-	-	-	-	-	-	3639.483
April	977.560	841.860	519.819	604.615	710.257	711.465	4367.929
May	529.208	442.269	267.392	304.905	364.195	375.570	2302.250
June	439.765	348.281	202.683	248.751	290.902	300.465	1841.333
July	535.509	430.647	248.066	305.671	360.245	372.539	2263.423
August	1198.067	1060.464	634.186	783.894	924.718	954.422	5555.050
September	958.408	840.156	506.865	592.455	714.762	741.661	4379.099
October	1055.134	939.065	84.936	749.812	840.779	841.025	4487.183
November	1076.843	975.241	0.000	803.520	867.807	843.861	4552.147
December	484.942	419.483	0.000	332.696	330.007	336.353	1927.980
TOTAL	**7255.436**	**6297.466**	**2463.947**	**4726.319**	**5403.672**	**5477.361**	**41033.667**

Table 11. WT system evaluation for 2011.

Month	Difference (kWh)	Difference (%)	System yield (kWh/kW)	Peak Power (kW)
January	-	-	58.906	34.000
February	-	-	99.922	34.050
March	-	-	101.097	34.660
April	-2.353	-0.054	121.331	33.690
May	-18.711	-0.819	63.951	33.410
June	-10.486	-0.573	51.148	32.320
July	-10.746	-0.477	62.873	31.880
August	0.701	0.013	154.307	28.390
September	-24.792	-0.569	121.642	32.410
October	23.568	0.522	124.644	29.220
November	15.125	0.331	126.449	29.770
December	-24.499	-1.287	53.555	29.770
TOTAL	**-52.193**	**-0.165**	**1139.824**	

As can be seen from the Tables above, the difference between the energy production as reported by the inverters and as reported by the monitoring system is approximately 0.165%, thus no unexpected losses are observed in the energy transfer from the WT installation to the building.

Figure 27 illustrates the measurements of Table 10. The differences in the produced energy per WT were expected, since the topomorphy and elevation of the hill that the WTs are installed varies, resulting in each WT being exposed to different wind speed profiles. As concluded from Table 10, the highest performing WT produced 7255.436 kWh and the lowest performing WT produced 4726.319 kWh, which is almost a 35% difference.

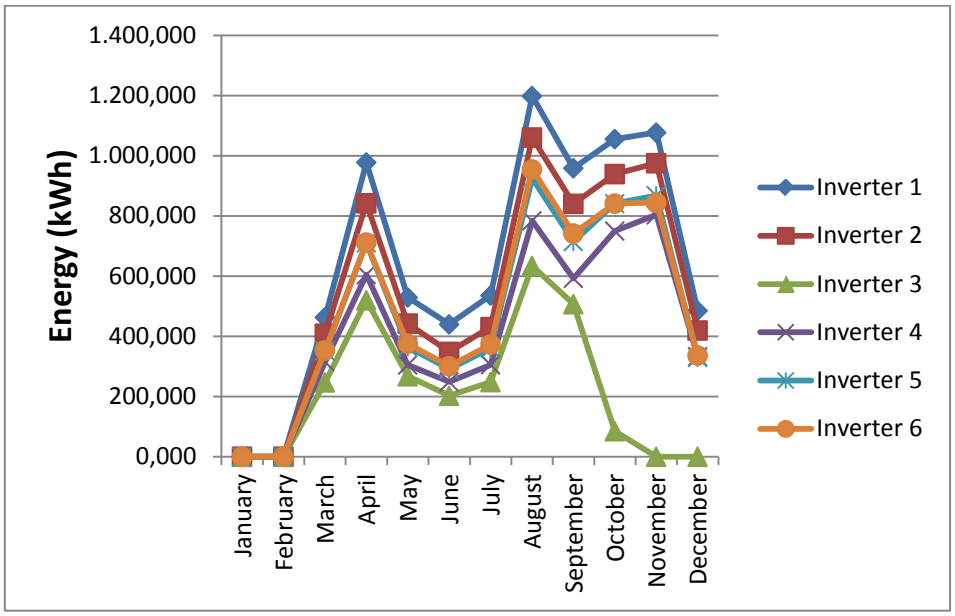

Figure 27. Energy produced per WT for 2011.

The WT system yield for 2011 is 1139.824 Kwh/kW, while total energy production during 2011 was 41033.667 kWh.

It can also be observed that, as expected, the energy production variations closely match the measured wind speed variations measured by the weather station. Higher energy producing period is from August to October.

It should also be noted that WT No3 exhibited increased wear at its main axle bearing and therefore it had to be put on brake to avoid further damage. This accounts for the fact that the measurements from October until December show minimal to zero energy production. More details are given in the maintenance section.

Similarly, Tables 12 and 13 present the same data for the period February to September 2012 as this is the most recent period.

Table 12. Energy produced by WT system from February to September 2012.

Month	Energy produced - Inverter 1 (kWh)	Energy produced - Inverter 2 (kWh)	Energy produced - Inverter 3 (kWh)	Energy produced - Inverter 4 (kWh)	Energy produced - Inverter 5 (kWh)	Energy produced - Inverter 6 (kWh)	Energy delivered to building (kWh)
February	585.041	367.129	268.470	332.853	389.769	389.106	2328.630
March	644.092	551.860	317.501	418.997	475.135	481.772	2878.900
April	391.830	299.875	163.869	234.907	242.553	262.821	1612.580
May	334.103	258.419	142.103	191.612	215.021	232.541	1376.110
June	1003.337	908.374	510.845	684.887	805.953	813.553	4740.750
July	784.650	680.240	384.604	504.532	584.074	597.041	3154.930
August	797.616	687.738	386.961	490.531	576.322	586.809	3356.370
TOTAL	**4540.669**	**3753.635**	**2174.353**	**2858.319**	**3288.827**	**3363.724**	**19448.270**

Table 13. WT system evaluation from February to September 2012.

Month	Difference (kWh)	Difference (%)	System yield (kWh/kW)	Peak Power (kW)
February	3.738	0.160	64.684	33.550
March	10.457	0.362	79.969	33.520
April	-16.725	-1.048	44.794	33.460
May	-2.311	-0.168	38.225	29.050
June	-13.801	-0.292	131.688	30.900
July	380.211	10.755	87.637	26.650
August	169.688	4.812	93.233	24.810
TOTAL	**531.257**	**2.659**	**540.230**	

Comparing the energy production values with the relevant period of 2011, it is clear that energy production is lower due to the less favorable meteorological conditions (i.e. lower wind speeds, also verified by Figure 22).

4.1.3.3 Maintenance and/or failures

The WT manufacturer advises a yearly maintenance plan for the WTs. The details of this plan are presented in the final section of this report, in the full-scale prototype plant maintenance manual.

During the maintenance activities, it was discovered that WT No3 exhibited abnormally high wear at its main axle bearing. To avoid further damage and for safety reasons the WT was stopped, while at the same time the manufacturer was informed of the situation. After evaluating the problem and under cooperation with both the local contractor and the WT manufacturer, the proposed solution was to completely replace the main axle and bearing assemblies. The whole repair procedure lasted approximately three months.

4.1.3.4 Conclusions

Given the measurements and calculated data, the WT system is performing adequately. However, the two main reasons for lower than expected energy production are the varying topomorphy of the installation location and the low wind speeds observed mainly during 2012. Stopping one of the WTs for approximately three months also impacted the overall energy production of 2011.

The problem that was encountered in this particular WT has been successfully dealt with and currently all WTs are operating normally. The problem served as an incentive to establish a new procedure to periodically check for increased noise and/or vibrations in the WTs to quickly detect any similar type of failure.

4.2 Full-scale demonstration building

4.2.1 Technical specifications

The demonstration building has been described in detail in section 2.2.1 therefore only the technical specifications of the building loads will be given below. More specifically, the technical specifications of the building's HVAC systems are presented in Tables 14 and 15 since these are the building's highest consumptions.

Table 14. VRV system technical specifications

Product Name		**PUHY-P350YHM-A(-BS)**
Power supply		3-phase 4-wire 400V 50/60 Hz
Cooling capacity	**kW**	40.0
COP		3.57
Temperature range (cooling – indoor)	**°C**	15-24
Temperature range (cooling – outdoor)	**°C**	-5 – 43
Heating capacity	**kW**	45.0
COP		3.72
Temperature range (heating – indoor)	**°C**	15-27
Temperature range (heating – outdoor)	**°C**	-20 – 15.5
Compressor		Inverter scroll hermetic
Refrigerant		R410A x 11.5 kgr

Table 15. Heat pump technical specifications

Power supply		3-phase 4-wire 380V 50 Hz
Cooling capacity	**kW**	50.0
Heating capacity	**kW**	55.0
Compressor		Double inverter scroll hermetic
Refrigerant		R410A

4.2.2 Measured parameters and calculations

Using the demonstration building's monitoring system the following magnitudes were measured for each type of load:

- Power consumption (kW)
- Energy consumption (kWh)

Subsequently, the recorded data were used to calculate:

- Total energy consumption for each type of load
- Annual energy consumption per building m^2
- Maximum and average power consumption for each type of load
- Peak load values and peak load duration

A basic building management scenario was established in order to represent office usage. Using the installed BMS, building operations were programmed as follows:

- Building lights turn on at 08:00 and turn off at 18:00
- HVAC turns on at 09:00 and turns off at 17:00
- Interior temperature setpoint is 21 ^{o}C (heating mode) and 26 ^{o}C (cooling mode)
- All consumptions are off during Saturdays and Sundays

Of course, different scenarios than the one described above were also tested but for limited periods.

Using the above measured and calculated data the distribution of energy between the building loads as well as the building's power consumption profile can be determined. Both are very important in order to implement a management strategy that can achieve higher energy savings and guarantee the sustained operation of the building.

The energy consumption according to the type of load is presented in Table 16 for the period February to September 2012 as this is the most recent period.

Table 16. Energy consumption data for each building load.

Month in 2012	HVAC (kWh)	VRV (kWh)	Lighting (kWh)	Other (kWh)
February	2197.73	3035.05	700.94	1175.84
March	1645.88	2956.58	685.33	1248.51
April	1569.32	816.97	895.55	1185.72
May	1316.92	1739.77	941.79	1238.14
June	2483.33	1585.51	851.78	1490.75
July	2529.48	1783.01	796.36	1311.49
August	836.76	2210.49	854.09	1221.01
September	1472.26	1245.79	503.47	1440.30
TOTAL	**14051.68**	**15373.17**	**6229.31**	**10311.76**

The building's total energy consumption for this period is 45965.92 kWh.

The consumed energy distribution according to type of building load is also displayed as a pie chart in Figure 28. It is clear that most of the energy is consumed to cover the building's cooling/heating needs (almost 64%), while the rest of the equipment and lighting loads account for approximately 22% and 14% respectively.

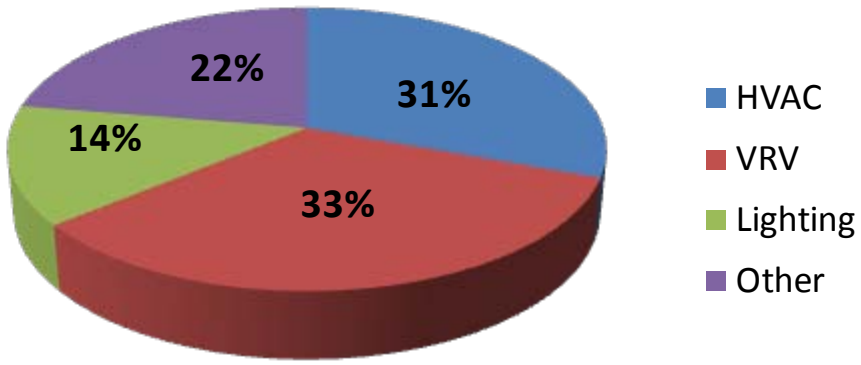

Figure 28. Consumed energy distribution for each building load.

Considering that the total surface area of the building is 525 m^2 and projecting the energy consumption figures to a yearly period, it is possible to calculate the building's annual energy consumption equal to 131.33 kWh/m^2/year.

The demonstration building's total power consumption profile for the period February to May 2012 is shown in Figure 29. As expected, the building's power consumption profile is largely dependent on the ambient conditions and seasonal changes as there is a distinctive drop in maximum load from March to April.

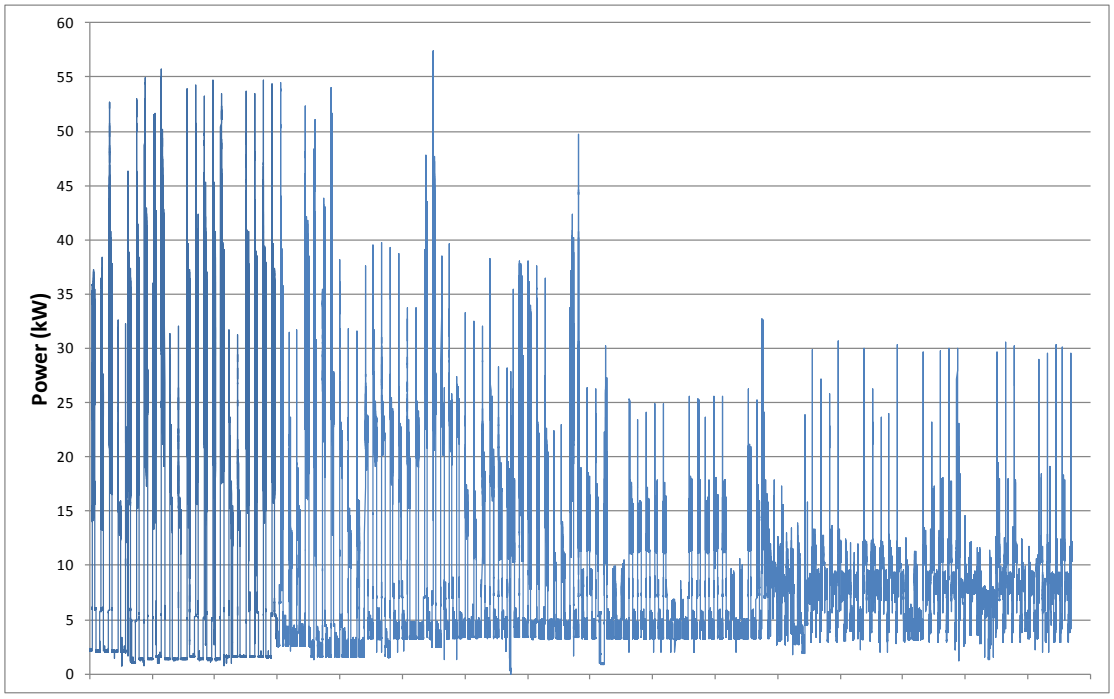

Figure 29. Building consumption profile.

By analyzing the average and maximum power consumptions on a monthly basis for each load separately, Table 17 is formed.

Table 17. Average and maximum power consumption per building load.

Month	HVAC (kW)		VRV (kW)		Lighting (kW)		Other (kW)	
	Average	Maximum	Average	Maximum	Average	Maximum	Average	Maximum
February	2.872	24.120	4.978	26.974	1.028	6.082	1.105	6.535
March	2.124	25.820	4.326	26.684	1.086	3.751	1.898	6.556
April	1.828	22.900	1.486	21.097	1.246	4.733	1.962	7.454
May	1.482	24.080	2.695	28.695	1.234	4.567	1.915	7.088
June	3.395	23.270	2.079	25.239	1.184	3.798	2.064	4.475
July	4.027	23.290	2.675	25.987	1.210	3.780	2.015	4.441
August	1.296	22.070	3.063	26.270	1.178	3.662	1.429	4.435
September	2.058	25.040	1.744	25.033	0.701	3.712	2.001	4.286

A peak power profile analysis has also been conducted so as to identify the peak load of the building as a whole as well as the duration for which this load occurs. Using the detailed consumption profile of the entire building, the analysis first calculated the building's average power consumption, on a monthly basis. Subsequently, any consumption that was higher than this average was characterized as a "peak". The duration of the peak was defined as the time period during which the load remained higher than the average. The statistical results of this analysis are shown in Table 18.

Table 18. Peak power profile analysis statistics.

Month	Average building load (kW)	Maximum peak building load (kW)	Average Peak Duration (min)
February	10.070	55.750	7.900
March	9.400	57.450	18.954
April	6.560	49.730	61.687
May	7.400	30.640	17.994
June	8.734	36.640	26.101
July	9.860	43.200	14.740
August	7.665	32.740	38.141
September	6.470	32.360	13.384

From these data it is concluded that the average building load varies from approximately 6.5 kW to 10 kW and that the maximum building load varies from approximately 30 kW to 57 kW. The variations are mainly attributed to the changes in the behavior of the HVAC and VRV systems in relation to the ambient temperature variations depending on the season.

It is interesting to note that the average building load can be covered using only the installed RES and more specifically the PV system whose energy production follows more predictable trends. On the other hand, it is possible that there are cases when the RES can not meet the maximum building load and then the micro-CHP FC is needed to supply the difference of missing power. It is also clear that a load balancing scheme is necessary in order to adjust the overall building consumption profile.

4.2.3 Maintenance and/or failures

The maintenance activities of the building have focused mainly on the HVAC systems (filter cleaning, leak detection, pressure checks, electrical checks etc) to ensure proper and efficient operation according to the manufacturer's guidelines. Maintenance of all firefighting measures (fire extinguishers, audio and visual alarms, push buttons etc) is also conducted on a regular basis.

4.2.4 Conclusions

Using the implemented monitoring system, it is possible to measure the consumption of energy according to type and location of load inside the demonstration building. This is very important because at the same time, it means that these loads can be controlled in order to balance the variations in the production – consumption equation.

The demonstration building annual consumption per m^2 is 131.33 kWh/m^2/year. From an energy point of view the installed RES are more than adequate to cover the building energy needs (yearly production from RES is approximately 110 MWh, while yearly consumption is approximately 70 MWh).

4.3 Electrolyser

The electrolyser's (EL) performance was evaluated based on data collected during the automatic operation of the full-scale RES-H_2 prototype system using the developed control algorithm. As described in the DoW, the goal of the evaluation was to determine the efficiency and the hydrogen production rate of the EL.

However, additional performance criteria were calculated such as the specific yield ratio (i.e. the amount of energy, in kWh, that is consumed for the production of 1 Nm^3 of H_2), the average and maximum power consumption and the time elapsed between EL start and H_2 feeding to the distribution grid. A short presentation of observations, made during the evaluation period, of other parameters that affect the operation of the EL is also part of the performance evaluation analysis.

4.3.1 Technical specifications

The EL is used to produce gaseous H_2 and its technical specifications are given in Table 19 below.

Table 19. Technical specifications of EL.

DESCRIPTION		VALUE
Rated H_2 production capacity	Nm^3/h	4
Outlet pressure (HP version)	barg	12
Hydrogen purity	% vol	99.3 – 99.8
Demi water consumption	l/h	3.4
Rated power consumption	kW/h	22.3

Since the produced H_2 purity is lower than the one required by the micro-CHP FC (something that would result in decreased performance), the EL is also supplemented by a H_2 purifier system. The technical specifications of the purifier are listed in Table 20.

Table 20. Technical specifications of DXH 12 purifier system.

DESCRIPTION		VALUE
Maximum H_2 Outlet Flow	Nm^3/h	12
Hydrogen purity	% vol	>99.999
Rated power	W	650

4.3.2 Measured parameters and calculations

Using the demonstration building's monitoring system as well as the internal logging capabilities of the EL, the following magnitudes were measured:

- Power consumption (kW)
- Energy consumption (kWh)
- H_2 pressure in the buffer storage (bar)

- H_2 pressure in the high pressure storage (bar)
- EL production factor (percentage of the EL maximum H_2 production rate of 4 Nm^3/h)

The production factor value is recorded in 10 sec intervals. All other magnitudes are recorded in 1 minute intervals.

Subsequently, the recorded data were used to calculate:

- Maximum and average power consumption
- Total energy consumption
- Actual production rate and total volume of produced H_2
- Total volume of actually stored H_2 in the pressure cylinder stacks
- Specific yield ratio
- EL efficiency

The analysis used data from several operational cycles of the EL under various conditions in order to be representative of real operating conditions. The calculation methodology and the assumptions that were made are presented below in detail.

4.3.2.1 Maximum and average power consumption

As already mentioned, the building's monitoring system measures the power consumption in 1 min intervals therefore calculating the maximum and average values is straightforward using the stored data.

4.3.2.2 Total energy consumption

Similarly, the building's monitoring system measures the cumulative energy consumption in 1 min intervals, therefore calculating the total energy consumption (is also easy through a simple subtraction of the stored values corresponding to the desired time period.

4.3.2.3 Volume of produced H_2

The calculation of the produced H_2 volume is based on the EL's production factor. The production factor is a percentage of the EL's maximum production rate (4 Nm^3/h) and its value is measured and stored by the EL internal logging system in 10 sec intervals. For example, if the production factor is 75 then during this 10 sec interval, the EL produced (75 / 100) * 4 = 3 Nm^3/h of H_2. Consequently, the volume of produced H_2 for a 10 sec interval is given by Equation 4:

(Equation 4)

, where

= volume of produced H_2 for the 10 sec interval

PF = EL production factor

Therefore, calculation of the total volume of produced H_2 corresponding to any desired time period is performed by summing the production factor values for all 10 sec intervals that make up this period.

(Equation 5)

, where

= volume of produced H_2

n = number of 10 sec intervals that make up the desired time period

4.3.2.4 Volume of stored H_2

As described in deliverable D7.1, H_2 is stored initially in a buffer (consisting of three pressure cylinders) and then fed to the compressor before being stored in the high pressure storage (consisting of four pressure cylinder stacks). Pressure in the buffer and high pressure cylinders is constantly measured and stored (in bar) and the total water capacities of the two storage stages are known (150 lt and 3480 lt respectively).

Therefore, in order to determine the volume of actually stored H_2 for any desired time period, the volume change in the buffer and storage should be calculated. This can be accomplished using the ideal gas law, under the assumptions that for the considered working pressures (below 200 bar), H_2 behaves as an ideal gas and that ambient temperature remains constant. Given these assumptions, the ideal gas law can be simplified to the form (isothermal process):

(Equation 6)

Applying the above equation for the buffer and storage and using P_1 = 1.01325 bar (atmospheric pressure), P_2 = known pressure after compression and V_1 = water capacity, the volume of stored H_2 is calculated as follows:

(Equation 7)

, where

= total volume of stored H_2

= volume of stored H_2 in buffer storage

= volume of stored H_2 in high pressure storage

= H_2 pressure in buffer storage until t_n (end of desired time period)

= H_2 pressure in buffer storage until t_0 (start of desired time period)

= H_2 pressure in high pressure storage until t_n (end of desired time period)

= H_2 pressure in high pressure storage until t_0 (start of desired time period)

4.3.2.5 Specific yield ratio

The specific yield ratio is determined by dividing the total energy consumed ($E_{consumed}$) with the volume of the produced H_2 by the electrolyser ($V_{H2producedtotal}$):

(Equation 8)

The specific yield ratio expresses the amount of electrical energy consumed by the EL to produce 1 Nm^3 of H_2. Obviously, the smaller this number is, the better.

4.3.2.6 Efficiency

When dealing with electrolysis, there are two efficiencies that are used to characterize the process. The first is the Faraday efficiency and the second is the energy efficiency. Faraday efficiency expresses how much of the current is converted in H_2 during the reaction and it is calculated as the ratio of the actually produced volume of H_2 to the volume of H_2 that should theoretically have been produced. Energy efficiency on the other hand, expresses how much energy is converted during the reaction and it is calculated as the ratio of the total electrical energy that it is consumed to the energy that is contained in the produced H_2.

This analysis focuses on the energy efficiency thus based on the above definition, the following equation is used for the calculation:

(Equation 9)

, where

(Equation 10)

HHV_{H2} = 12.7 MJ/m^3

4.3.3. Results and discussion

The results from two different EL operation cycles are summarized in Table 21.

Table 21. EL operation cycles results.

Operation cycle duration (mins)	Maximum power consumed (kW)	Average power consumed (kW)	Energy consumed (kWh)	H2 produced (Nm3)	H2 stored (Nm3)	H2 losses (Nm3 / %)	Specific yield (kWh/Nm3)	Efficiency (%)
300	23,920	19,987	99,946	14,752	14,218	0,534 / 3,621	6,775	52,069
225	24,750	19,923	74,788	11,075	10,833	0,242 / 2,188	6,753	52,242

As can be seen, the EL's specific yield is close to 6.76 kWh/Nm^3 and its efficiency is 52%. The H_2 losses are between 2 – 4% of the produced H_2.

Using the longest operation cycle data, Figure 30 presents variation of the production factor versus time. As can be seen in the Figure below, the EL needs approximately 2 mins to reach a stable production factor for this operation cycle (approximately 80%).

Also, two distinct phases of operation can be identified: the first lasts approximately 25 mins and is characterized by a stable production rate, while the second lasts for the remaining duration of the operation cycle (approximately 276 mins), where the production rate exhibits larger variation (minimum value is 67% - maximum value is 87%). During the first phase, the EL stable production factor is explained by the fact that the buffer storage needs to be filled and this takes approximately 25 mins. After that point, the H_2 compressor starts operating, which causes the H_2 pressure in the buffer storage to vary according to the compression rate, resulting to the variations observed to the EL's production factor.

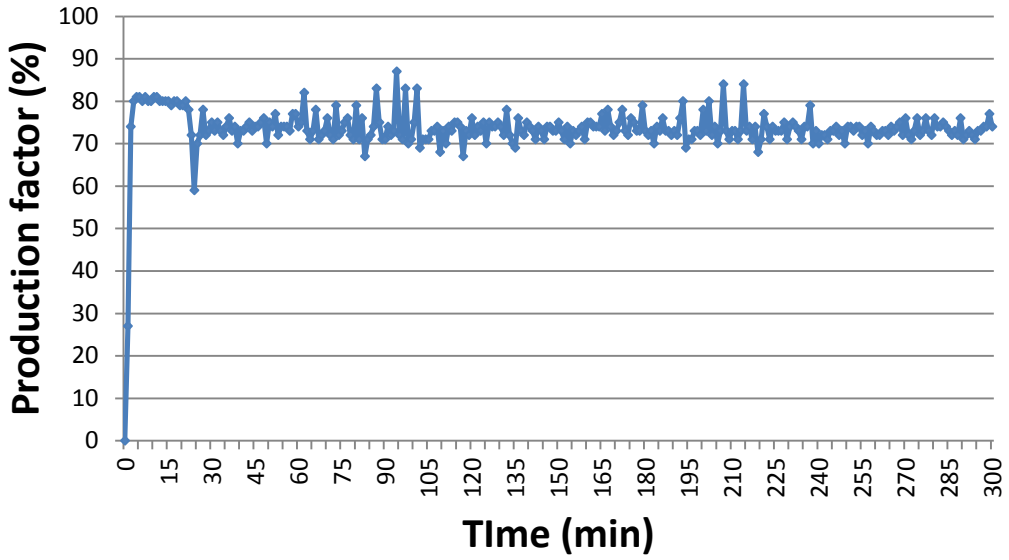

Figure 30. Production factor vs time.

Figure 31 shows the cumulative produced H_2 volume (in red) and cumulative stored H_2 volume (in blue) versus time.

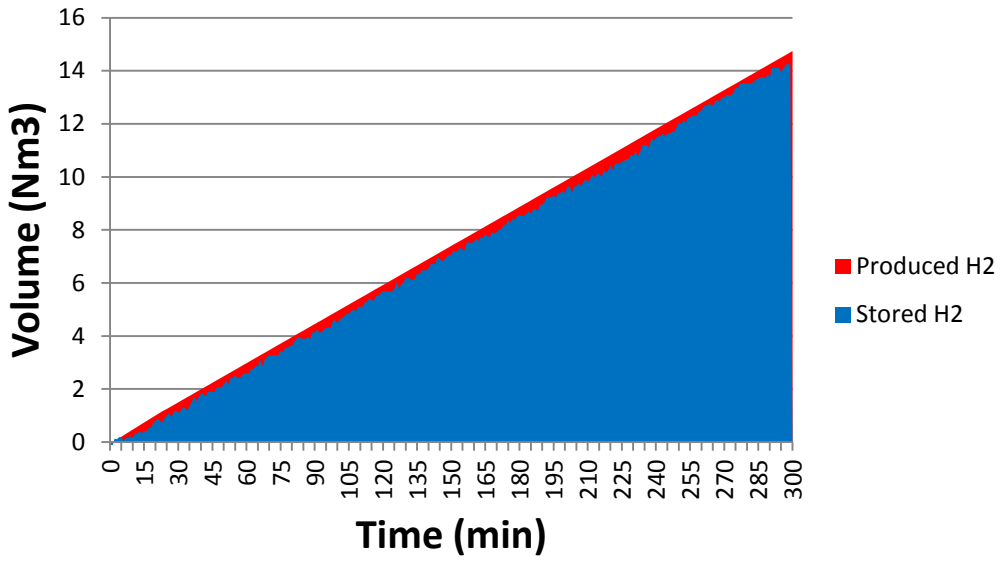

Figure 31. H_2 volumes vs time.

According to the measurements, the H_2 production rate is almost constant and is denoted by the linear variation of the produced H_2 volume versus time.

The measured differences between the produced and stored H_2 quantities are due to losses. These losses can be identified as follows:

- H_2 that is vented from the EL at the end of the operation cycle (the H_2 that is inside the EL stack is depressurized and released outside the demonstration building).
- H_2 that is also vented during the operation cycle, in very small quantities, in order to maintain the proper pressure inside the electrolyser.
- H_2 losses that occur at the compressor.

It should be noted that for operation cycles with shorter duration (30 to 60 mins), the percentage of H_2 losses can be much higher (up to 10 – 12%), due to the fact that the ratio of H_2 found inside the EL (which will be vented at the end of the operation cycle) to the totally produced H_2 is bigger.

4.3.4 Maintenance and/or failures

There was no need for EL maintenance according to the manufacturer's maintenance schedule during this period. There were also no signs of abnormal operation or failures that would justify earlier maintenance and/or repair actions.

It should be mentioned that there was only one occurrence when the EL did not manage to start operation due to low electrolyte temperature that was caused by very low ambient temperatures (close to 4 ^{0}C) during February. However, this behavior is normal since such low temperatures are out of of the operating environmental conditions range of the EL's specifications. It must also be taken into account that such temperatures are rarely experienced in Lavrion's area, therefore no further corrective action was taken to deal with this extreme case.

4.3.5 Conclusions

Based on the calculations, the EL's performance figures are in agreement with what is reported in the literature (Zittel and Wurster, 1996), although they are on the lower end of the range.

4.4 Micro-CHP FC

The micro-CHP FC performance was evaluated based on data collected during the automatic operation of the full-scale RES-H_2 prototype system using the developed control algorithm. As described in the DoW, the goal of the evaluation was to determine the hydrogen consumption, electrical and thermal energy production and efficiencies of the micro-CHP FC.

However, additional performance criteria were calculated such as H_2 losses and the response times needed from start of operation until energy is fed to the building and from start of operation until maximum power is achieved.

4.4.1 Technical specifications

The micro-CHP FC is based on PEM technology to produce electrical and thermal energy. The produced DC current is transformed to AC and is directly fed to the demonstration building, while the hot water is stored in the HRS to be used when needed. The micro-CHP FC technical specifications are given in Table 22 below.

Table 22. Technical specifications of the micro-CHP FC.

DESCRIPTION		VALUE
Electrical power production	kW	6-20
Thermal power production	kW	5-20
Maximum Hydrogen consumption	Nm^3/h	22
Maximum Hydrogen inlet pressure	bar	1
Demi water conductivity	μs/cm	<1
Hot water flow rate	Nm^3/h	1-4

4.4.2 Measured parameters

Using the demonstration building's monitoring system as well as the internal logging capabilities of the FC, the following magnitudes were measured:

- Power consumption (kW)
- Energy consumption (kWh)
- H_2 pressure in the high pressure storage (bar)
- Power production by FC (kW)
- Energy production by FC (kWh)
- H_2 consumption by FC (Nm^3/h)
- Water temperature inside the HRS "puffer" tank (^0C)

The first three magnitudes are recorded in 1 min intervals. All other magnitudes are recorded in 5 sec intervals.

Subsequently, the recorded data were used to calculate:

- Actual consumption rate and total volume of consumed H_2
- Electrical and thermal energy produced by FC
- Specific yield ratio
- FC electrical and thermal efficiencies

The analysis used data from several operational cycles of the FC under various conditions in order to be representative of real operating conditions. The calculation methodology and the assumptions that were made are presented below in detail.

4.4.2.1 Volume of consumed H_2 from the high pressure storage

The micro-CHP FC uses the gaseous H_2 that is stored in the high pressure storage. As already described, the pressure is constantly measured and stored (in bar) and the total water capacity of this storage stage is known (3480 lt).

Therefore, in order to determine the volume of actually consumed H_2 for any desired time period, the volume change only in the high pressure storage should be calculated. Using the same assumptions as in the case of the EL (for working pressures below 200 bar H_2 behaves as an ideal gas and that ambient temperature remains constant) Equation 7 is modified as follows:

(Equation 11)

, where

= volume of consumed H_2 from high pressure storage

= H_2 pressure in high pressure storage until t_n (end of desired time period)

= H_2 pressure in high pressure storage until t_0 (start of desired time period)

4.4.2.2 Volume of consumed H_2 by the FC stack

The calculation of the consumed H_2 volume by the FC stack is based on the micro-CHP's internal measurement of the H_2 consumption rate. This value is measured and stored in Nm^3/h units by the FC's internal logging system in 5 sec intervals. Consequently, the volume of consumed H_2 for a 5 sec interval is given by Equation 12:

(Equation 12)

, where

= volume of consumed H_2 for the 5 sec interval

CR = H_2 consumption rate

Therefore, calculation of the total volume of consumed H_2 by the FC corresponding to any desired time period is performed by summing the H_2 consumption rate values for all 5 sec intervals that make up this period.

(Equation 13)

, where

= volume of consumed H_2

n = number of 5 sec intervals that make up the desired time period

4.4.2.3 Electrical energy produced

The electrical energy that is produced by the micro-CHP is calculated using the stack current and stack voltage measurements of the FC's internal logging system and taking into account the duration of the time period. Again, since these measurements are recorded in 5 sec intervals, the calculation for is as follows:

(Equation 14)

, where

= produced electrical energy

V_i = stack voltage of the i-ith interval

I_i = stack current of the i-ith interval

n = number of 5 sec intervals that make up the desired time period

4.4.2.4 Thermal energy produced

As already mentioned, the thermal energy that is produced by the micro-CHP heats the water that is circulated and stored in the HRS "puffer" tank. The calculation of the produced thermal energy is based on the following equation:

(Equation 15)

, where

= produced thermal energy

m = the water mass, which is known and equal to 850 kgr

c_p = water specific heat
ΔT = the temperature difference of the water

The only unknown parameter in Equation 18 is the water temperature inside the HRS "puffer" tank, which is measured using thermocouples. Specifically, two thermocouples are installed in the tank (one close to the top and one close to the bottom) and the water temperature used in the calculation is the average of these two measurements.

4.4.2.5 Specific yield ratio

The specific yield ratio in the case of the FC is determined by dividing the total electrical energy produced with the volume of the consumed H_2 by the FC ( ). It should be noted that since the micro-CHP also consumes a portion of electrical energy, only the net electrical energy is used in the calculation:

(Equation 16)

The specific yield ratio expresses the net amount of electrical energy produced by the FC after consuming 1 Nm^3 of H_2. Obviously, the higher this number is, the better.

4.4.2.6 Electrical efficiency

The electrical efficiency is calculated as the ratio of the total electrical energy that is being produced to the energy that is contained in the consumed H_2. It should be noted that since the micro-CHP also consumes a portion of electrical energy, only the net electrical energy is used in the calculation.

(Equation 17)

, where

(Equation 18)

$HHV_{H2} = 12.7\ MJ/m^3$

4.4.2.7 Thermal efficiency

Similar to the electrical efficiency, the thermal efficiency is calculated as the ratio of the total thermal energy that is being produced to the energy that is contained in the consumed H_2.

(Equation 19)

4.4.3. Results and discussion

The results from two different micro-CHP FC operation cycles are summarized in Tables 23a and 23b.

Table 23a. Micro-CHP FC operation cycles results.

Operation cycle duration (mins)	Energy consumed (kWh)	Electrical energy produced (kWh)	Thermal energy produced (kWh)
60	0,002	7.659	7.461
60	0,002	8.385	8.153

Table 23b. Micro-CHP FC operation cycles results.

H2 consumed from storage (Nm3)	H2 consumed from FC (Nm3)	H2 losses (Nm3 / %)	Specific yield (kWh/Nm3)	Electrical Efficiency (%)	Thermal Efficiency (%)
5.942	4.635	1.307 / 21.991	1.652	46.826	45.630
6.629	5.149	1.480 / 22.320	1.628	46.149	44.884

As can be seen, the FC's specific yield is approximately 1.64 kWh/Nm^3, its electrical efficiency is 46% and its thermal efficiency is close to 45%, resulting in overall efficiency of approximately 91%.

At the same time, H_2 consumption for the reported operation cycles (the micro-CHP was mostly operating at 10 kWel) is approximately 6.3 Nm^3/h, which is much better than the technical specifications that called for approximately 10 Nm^3/h at this power level. What is even more interesting is that the H_2 losses (mainly due to the periodic venting that takes place during operation) are as high as 22%, which means that there might be potential room for improvement in this aspect of FC operation.

Figure 32 presents the electrical power produced by the micro-CHP versus time during a typical operation cycle. The starting point of this Figure matches the time when the EMCS gives the command to the micro-CHP to start operation. As can be seen, the micro-CHP needs approximately 3 mins to start feeding power to the building and approximately 5 mins to achieve maximum power of 10 kW.

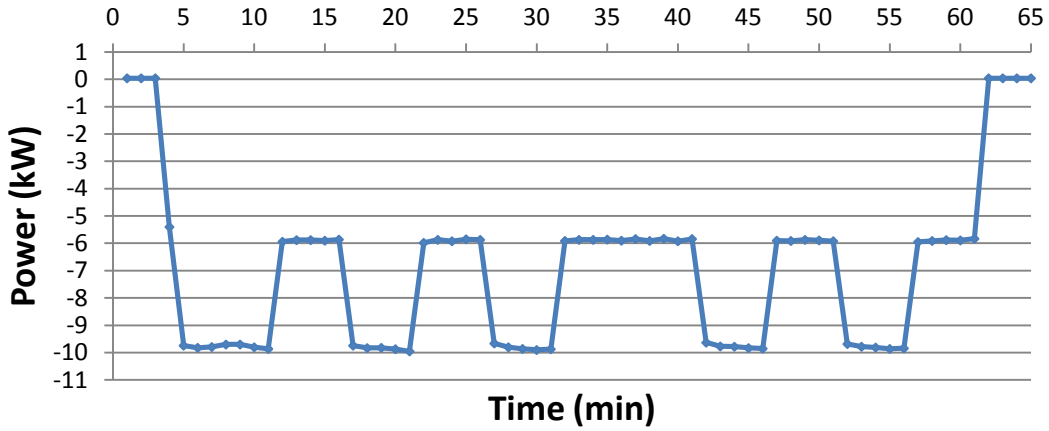

Figure 32. Production factor vs time.

The observed power production pattern that involves changes at the power setpoint of the micro-CHP is determined by the commands issued from the EMCS according to the balance of energy in the entire system. When the energy shortage becomes higher (i.e. more energy is needed to achieve equilibrium) the micro-CHP has to operate at a higher setpoint and vice-versa.

Figure 33 shows the cumulative consumed H_2 volume by the FC (in red) and cumulative consumed H_2 volume from the storage (in blue) versus time. As already discussed, there are significant losses due to H_2 venting.

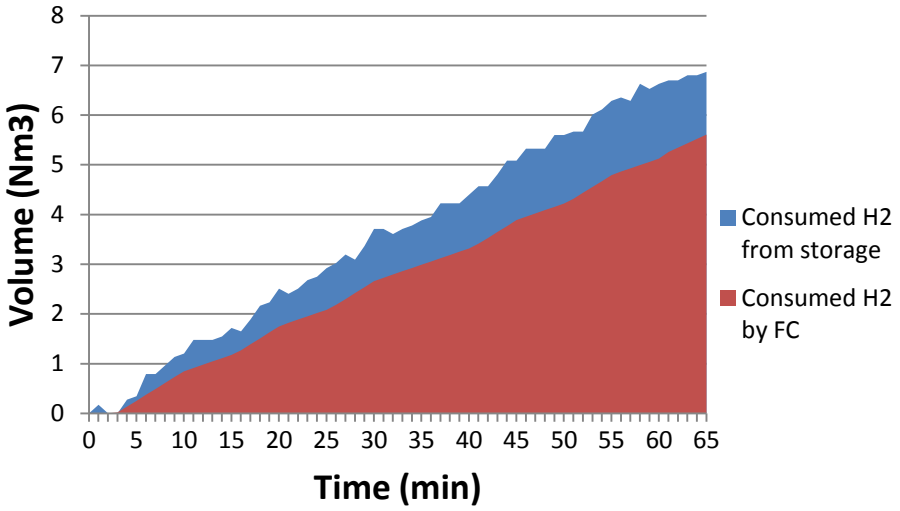

Figure 33. H_2 volumes vs time.

4.4.4 Maintenance and/or failures

During the commissioning of the micro-CHP there have been cases of warning messages and alarms but after close cooperation between NTUA and ICI Caldaie, they were successfully dealt with. The main causes were identified in the synergistic

operation between micro-CHP and the DC/AC inverter, the control of water temperature in order to achieve the steady-state in shorter time and the proper ventilation of the micro-CHP cabinet.

Furthermore, after several months of problem-free operation, there were measurements that indicated lower than expected stack voltage. A full test of the micro-CHP was conducted by ICI Caldaie and it was found that one of the two stacks used in the FC showed signs of possible membrane rupture in a set of cells. In order to avoid further damage to the unit and to guarantee the safety of the installation, the FC continued to operate at lower power setpoints until it could be repaired. The damaged stack was finally replaced with a new one of the exact same type and is currently fully operational.

The periodic maintenance of the FC mainly involves checking of all connections and valves for leaks. It also involves activities regarding the installed peripherals such as periodic measurements of the water conductivity produced by the demineralization system, checking of the filter in the air blower, inspection electrical connections and power supply to the control cabinet etc.

4.4.5 Conclusions

The performance analysis verifies that the micro-CHP FC achieves the targets set (electrical efficiency higher than 40%, total efficiency higher than 90%, H_2 consumption less than 20 Nm^3/h). Given the observed H_2 losses, it is very likely that even better results can be achieved.

It should also be noted that considerable tuning of the operation parameters were required as well as integration issues had to be solved in order to adjust the FC operation to achieve these goals.

4.5 H_2 Burner

The H_2 Burner was developed to operate using only gaseous H_2 with the goal of producing heat through the combustion of H_2 and transfer it to the HRS in the form of hot water.

The H_2 Burner performance was evaluated based on data collected during the automatic operation of the full-scale RES-H_2 prototype system using the developed control algorithm. The goal of the evaluation was to determine the hydrogen consumption, thermal energy production and specific yield.

4.5.1 Technical specifications

The Hydrogen Burning System consists of two main components namely the H_2 Burner and the condensing boiler. The technical specifications are given in Table 24 below.

Table 24. Technical specifications of the Hydrogen Burning System.

DESCRIPTION		VALUE
H_2 inlet pressure	mbar	20-50
Maximum H_2 consumption	Nm^3/h	21
Thermal power production	kW	50-90

4.5.2 Measured parameters

Using the demonstration building's monitoring system as well as the internal logging capabilities of the FC, the following magnitudes were measured:

- Power consumption (kW)
- Energy consumption (kWh)
- H_2 pressure in the high pressure storage (bar)
- Water temperature inside the HRS "puffer" tank (^0C)

The first three magnitudes are recorded in 1 min intervals, while the water temperature is recorded in 5 sec intervals.

Subsequently, the recorded data were used to calculate:

- Actual consumption rate and total volume of consumed H_2
- Thermal energy produced
- Specific yield ratio

The analysis used data from several operational cycles of the H_2 Burner under various conditions in order to be representative of real operating conditions. The calculation methodology and the assumptions that were made are presented below.

4.5.2.1 Volume of consumed H_2 from the high pressure storage

Similar to the micro-CHP, the H_2 Burner uses the gaseous H_2 that is stored in the high pressure storage. As already described, the pressure is constantly measured and stored (in bar) and the total water capacity of this storage stage is known (3480 lt) so Equation 11 (section 4.4.2.1) can be directly applied to calculate the volume of consumed H_2.

4.5.2.2 Thermal energy produced

The thermal energy that is produced by the H_2 Burner heats the water that is eventually circulated and stored in the HRS "puffer" tank. Again, the calculation of the produced thermal energy is based on Equation 15 that has already been described in section 4.4.2.4.

4.5.2.3 Specific yield ratio

The specific yield ratio is determined by dividing the total thermal energy produced with the volume of the consumed H_2 by the Burner. Equation 8 (section 4.3.2.5) can be directly applied.

The specific yield ratio expresses the net amount of thermal energy produced by the H_2 Burner after consuming 1 Nm^3 of H_2. Obviously, the higher this number is, the better.

4.5.3. Results and discussion

The results from two different H_2 Burner operation cycles are summarized in Table 25.

Table 25. H_2 Burner operation cycles results.

Operation cycle duration (mins)	Electrical energy consumed (kWh)	Thermal energy produced (kWh)	H2 consumed from storage (Nm3)	Specific yield (kWh/Nm3)
50	0,375	10.871	9.033	1.203
33	0,248	7.313	6.079	1.203

As can be seen, the H_2 Burner's consumption rate is approximately 11 Nm^3/h and its specific yield is 1.203 kWh/Nm^3.

To further analyze the performance of the H_2 Burner, Figure 34 presents the water temperature inside the HRS tank versus time during the 1st operation cycle.

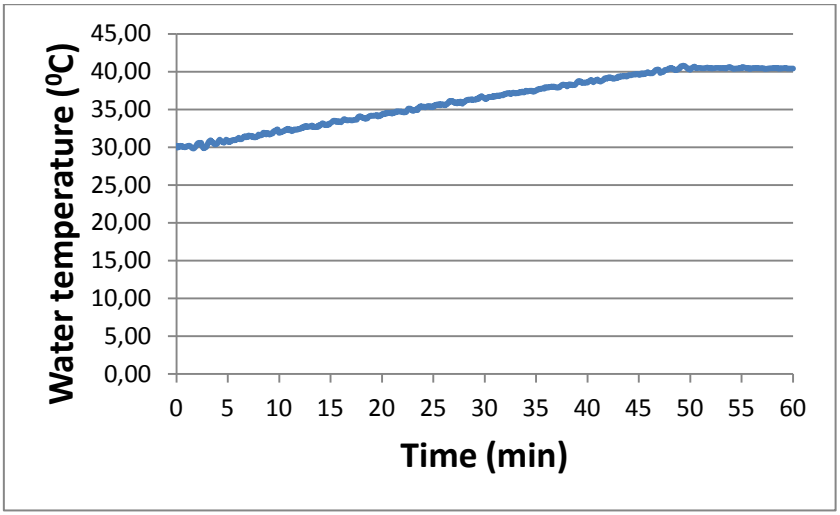

Figure 34. Water temperature vs time.

From this diagram, it can be concluded that the H_2 Burner needs approximately 45 mins to raise the temperature of 850 kgr of water by 10 ^0C.

Figure 35 shows the cumulative consumed H_2 volume versus time.

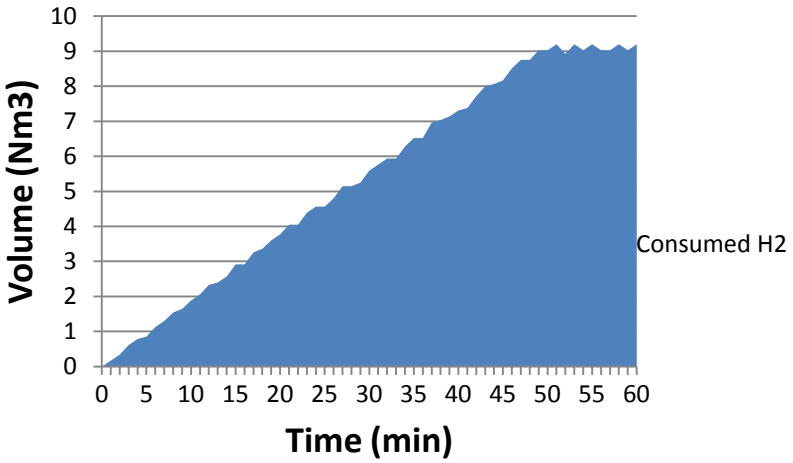

Figure 35. H_2 volume consumption vs time.

4.5.4 Maintenance and/or failures

The periodic maintenance of the H_2 Burner mainly involves checking of all connections for leaks and checking for proper condensation drainage. No failures have occurred since the commissioning of the H_2 Burner.

4.5.5 Conclusions

In order to complete the performance evaluation, an analysis of the energy consumption savings achieved in the building's HVAC system through the use of the H_2 Burner to pre-heat the water is currently conducted. The preliminary results show that the H_2 Burner and HRS synergistic operation is feasible enabling the integration of H_2 with HVAC systems based on water to air heat exchangers and heat pumps. Furthermore, there were no major differences in the overall energy consumption.

4.6 H_2 Compressor

The H_2 Compressor performance was evaluated based on data collected during the automatic operation of the full-scale RES-H_2 prototype system using the developed control algorithm. The goal of the evaluation was to determine the average and maximum power consumption, the specific energy consumption as well as the average and maximum compressor capacity.

4.6.1 Technical specifications

The technical specifications of the H_2 Compressor are given in Table 26.

Table 26. Technical specifications of the H_2 Compressor.

DESCRIPTION		VALUE
Maximum power consumption	kW	13.6
Maximum delivery pressure to compressor	bar	18
H2 delivery temperature to compressor	^{0}C	30-40
Maximum design outlet pressure	bar	400
Maximum design outlet temperature	^{0}C	65
Compressor capacity (@ 10 bar)	Nm^3/h	3.6
Stages		1

4.6.2 Measured parameters

Using the demonstration building's monitoring system the following magnitudes were measured (recorded in 1 min intervals):

- Power consumption (kW)
- Energy consumption (kWh)
- H_2 pressure in the high pressure storage (bar)
- H_2 pressure in the buffer storage (bar)

Subsequently, the recorded data were used to calculate:

- Average and maximum power consumption
- Total and specific energy consumption
- Average and maximum compressor capacity
- Volume of compressed H_2

The analysis used data from several operational cycles of the H_2 Compressor under various conditions in order to be representative of real operating conditions. The calculation methodology and the assumptions that were made are presented below.

4.6.2.1 Maximum and average power consumption

As already mentioned, the building's monitoring system measures the power consumption in 1 min intervals therefore calculating the maximum and average values is straightforward using the stored data.

4.6.2.2 Total energy consumption

Similarly, the building's monitoring system measures the cumulative energy consumption in 1 min intervals, therefore calculating the total energy consumption is also easy through a simple subtraction of the stored values corresponding to the desired time period.

4.6.2.3 Average and maximum compressor capacity

As already described, H_2 is stored initially in a buffer (consisting of three pressure cylinders) and then fed to the compressor before being stored in the high pressure storage (consisting of four pressure cylinder stacks). Pressure in the buffer and high pressure cylinders is constantly measured and stored (in bar) and the total water capacities of the two storage stages are known (150 lt and 3480 lt respectively).

Therefore, in order to determine the compressor capacity (i.e. compression rate) for any desired time period, the volume change rate in the buffer should be calculated by determining the volume changes for small time intervals. Using the same assumptions as in the case of the EL (for working pressures below 200 bar H_2 behaves as an ideal gas and that ambient temperature remains constant) Equation 7 is modified as follows:

(Equation 20)

, where

= volume change in buffer

= H_2 pressure in buffer storage until t_n (end of desired time period)

= H_2 pressure in buffer storage until t_0 (start of desired time period)

Calculating the average and maximum compression capacities is then straightforward.

4.6.2.4 Volume of compressed H_2

A similar method of calculation is used to calculate the total volume of compressed H_2, taking into consideration that the compressed H_2 is stored in the high pressure storage section. Therefore:

(Equation 21)

, where

= total volume of compressed H_2

= H_2 pressure in high pressure storage until t_n (end of desired time period)

= H_2 pressure in high pressure storage until t_0 (start of desired time period)

4.6.2.5 Specific energy consumption

The specific energy consumption is determined by dividing the total energy consumed ($E_{consumed}$) with the total volume of compressed H_2 ( ):

(Equation 22)

The specific energy consumption expresses the amount of electrical energy consumed by the EL to compress 1 Nm^3 of H_2. Obviously, the smaller this number is, the better.

4.6.3. Results and discussion

The results from two different H_2 Compressor operation cycles are summarized in Table 27.

Table 27. H_2 Compressor operation cycles results.

Operation cycle duration (mins)	Maximum power consumed (kW)	Average power consumed (kW)	Energy consumed (kWh)	H2 compressed (Nm3)	Specific energy (kWh/Nm3)	Maximum compressor capacity (Nm3/h)	Average compressor capacity (Nm3/h)
362	2.370	1.454	8.823	15.799	0.558	3.847	2.619
469	2.530	1.467	11.437	20.264	0.564	3.847	2.592

As can be seen, the H_2 Compressor average capacity rate is approximately 2.6 Nm^3/h, almost matching the production rate of the EL. The H_2 Compressor consumes close to 0.55 kWh of electrical energy in order to compress 1 Nm^3 of H_2.

Figure 36 presents the compressor capacity variations versus time for the 1st operation cycle.

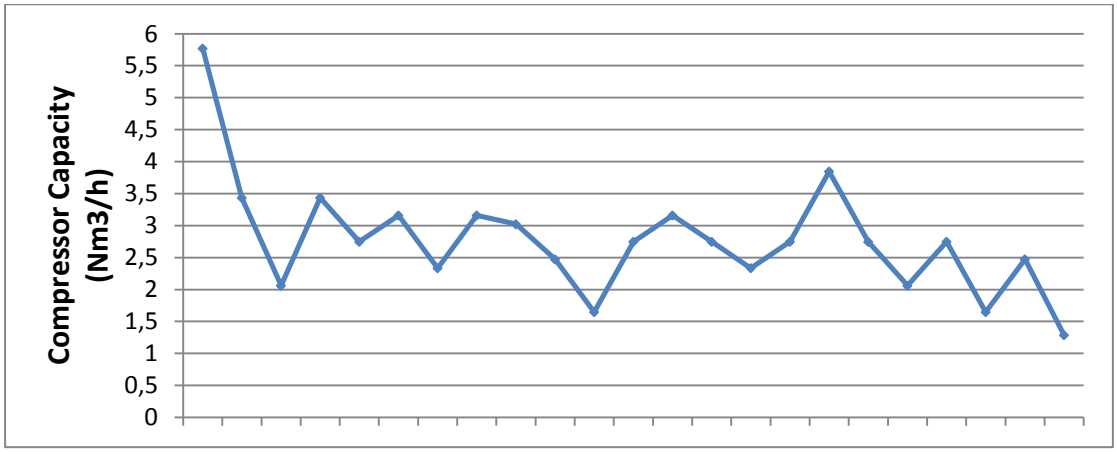

Figure 36. Compressor capacity vs time.

The reason for the variations in the compressor capacity is that initially the buffer storage is almost full, so the compressor has enough H_2 at its inlet and therefore at

the start of compressor operation the capacity is higher. After the H_2 in the buffer is compressed, the capacity is adjusted by the production rate of the EL and the pressure differences between the EL outlet and compressor inlet.

4.6.4 Maintenance and/or failures

As described in section 2.3, there were extensive maintenance activities carried out in the H_2 Compressor before and during its installation for the full-scale of the demonstration plant.

Periodic maintenance from them on, include the checking of oil levels and the checking for any possible leaks either in the closed water cooling circuit or the connections to the H_2 distribution grid.

4.6.4 Conclusions

The two most important conclusions resulting from the performance evaluation of the H_2 Compressor are the calculation of the specific energy consumption and the detailed calculation of the capacity variations. Using this information it is possible to optimize the buffer pressure setpoint for which the compressor starts operating and therefore optimize the synergistic operation with the EL. It is concluded that this setpoint should correspond to approximately 6 bars, thus guaranteeing the initial maximum capacity of the compressor and the sustained operation of the EL at high production rates.

4.7 RES-H_2 hybrid energy system

The full-scale RES-H_2 prototype system performance was evaluated based on data collected during the automatic operation using the developed control algorithm. The goal of the evaluation was to determine the efficiency of the system and to investigate the Zero Energy Building (ZEB) operation of the demonstration plant.

It should be noted that considerable efforts have been made both from IKERLAN and NTUA for the development of the the control algorithm and the optimization of its parameters until it reaches its final form. Since it was not possible to examine the operation of the demonstration plant for extensive time periods for every change that was introduced in the control algorithm, a mixed approach of simulation and operation under real conditions was adopted.

The modifications that were finally introduced in the control algorithm are:

- The equipment start/stop commands are issued based on the cumulative value of the SOC instead of the value of the SOC during the last 5 min interval.
- The cumulative SOC value is reset at predetermined time periods.
- The equipment power setpoints are calculated dynamically based also on the actual quantity of stored H_2. For example, in case that the storage level is high and there is excess of energy, the EL operation setpoint is kept low. In

the opposite case, if the storage level is low and there is shortage of energy, the FC operation setpoint is kept low.

The different behavior of the control algorithm before and after the above modifications are presented in Figures 37a to 37b. In these figures, the red line represents operation of the demonstration plant using the control algorithm and the pink line represents operation without any kind of control.

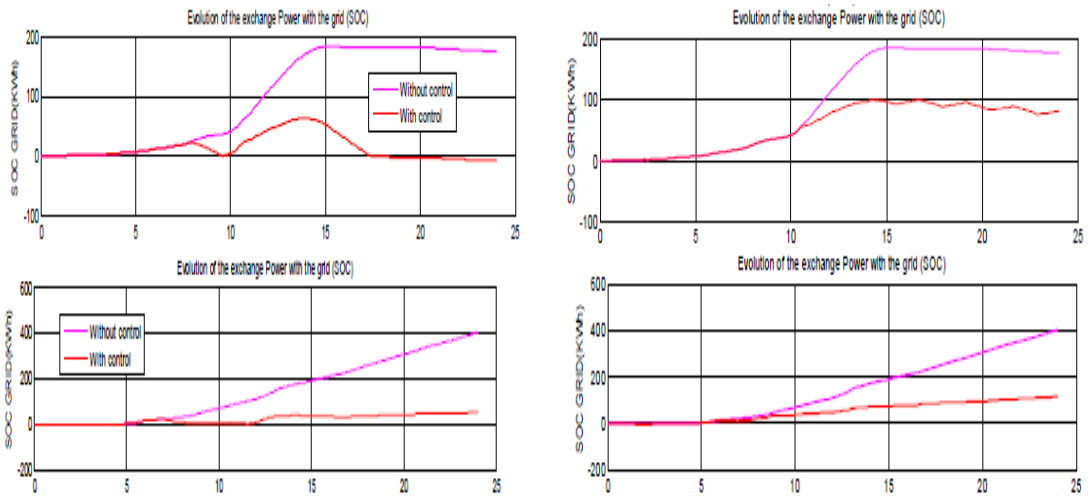

Figure 37a. Differences in control algorithm behavior regarding energy exchange with the grid (left modified, right original) in case of excess energy.

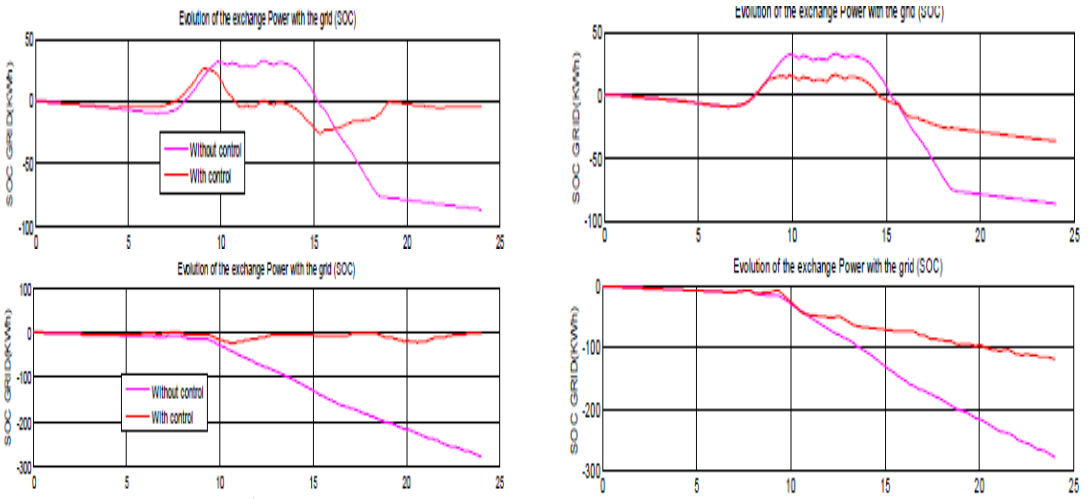

Figure 37b. Differences in control algorithm behavior regarding energy exchange with the grid (left modified, right original) in case of energy shortage.

4.7.1 Methodology

In order to calculate the efficiency of the full-scale RES-H_2 system, an energy balance was conducted in order to identify the energy that is being given to the system and the energy that is being taken from the system, since according to the definition of efficiency the following equation applies:

(Equation 23)

Further analyzing the components of Equation 23, it is clear that the energy that is being taken from the system is the electrical energy that is produced by the micro-CHP FC plus the thermal energy that is produced by the micro-CHP FC and the H_2 Burner:

(Equation 24)

Similarly, the energy that is being given to the H_2 system is the energy that is being produced from the RES minus the energy that is consumed by the demonstration building according to how they have been calculated in the relevant sections of this deliverable:

(Equation 25)

It should be noted that the energy exchange with the public power grid (can be either taken from or given to the system and is therefore used either in Equation 24 or Equation 25 depending on the case.

It should also be noted that normally the energy contained in the H_2 should be taken into consideration. However, the energy balance is performed for time periods that correspond to zero change in the volume of stored H_2 and therefore this factor is not included in the above equations.

Finally, it was necessary for each selected time period to include the operation of every system component. This way the calculated efficiency would represent the entire system and not only portions of it and would therefore correspond to the lower possible efficiency that the system achieves.

Figure 38 gives a graphic representation of the way that the efficiency is calculated.

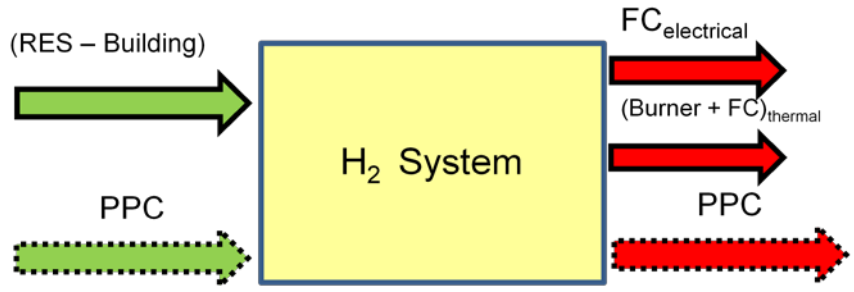

Figure 38. Efficiency calculation graph.

The efficiency calculation used data from several time periods in order to be representative of real operating conditions.

4.7.2. Results and discussion

The results from two different time periods are summarized in Table 28.

Table 28. Energy balance in the full-scale RES-H_2 system.

Energy production from RES (kWh)	Energy consumption from Building (kWh)	Energy exchange with PPC (kWh)	Electrical energy from FC (kWh)	Thermal energy from FC and Burner (kWh)	Efficiency (%)
239.397	196.087	-115.922	17.175	12.405	18.577
207.956	189.068	-146.211	17.488	8.247	15.588

As can be seen, the overall system efficiency varies from approximately 15% to 18%. As concluded from the data, this variation is due to the differences in the produced thermal energy.

If the thermal energy is excluded from Equation 24, which would correspond to a system without the HRS (no heat recovery ability), then the efficiency of the system would be equal to 10.786% and 10.592% respectively for each time period.

The primary objective of the developed RES-H_2 hybrid energy system was to achieve the ZEB target. In other words, the energy exchange with the grid should ideally be zero (the amount of electrical energy that is taken from the grid should be equal to the amount of energy that is given to the grid). Table 29 presents these data on a monthly basis for the entire full-scale demonstration plant (building, H_2 equipment and peripherals).

Table 29. Energy exchange of the full-scale demonstration plant and the grid.

Month	Energy given to PPC (kWh)	Energy taken from PPC (kWh)	Difference (kWh)
March	3.153,70	3.922,42	-768,72
April	2.779,26	3.535,01	-755,75
May	2.432,40	4.967,30	-2.534,90
June	3.524,00	2.514,10	1.009,90
July	2.951,80	3.112,07	-160,27
August	3.734,39	1.965,18	1.769,21
September	2.891,28	2.950,98	-59,70
October	2.208,92	2.205,62	3,30
TOTAL	**23.675,75**	**25.172,68**	**-1.496,93**

As can be seen, taking into consideration the entire period the system is very close to achieving the ZEB target. This is also supported by examining July, September and October of 2012 individually, during which the energy exchange with the grid is minimal and almost zero.

5. CONCLUSIONS

The conclusions that can be drawn based on the above results as well as the experience gained during the design, installation and operation phases of the full-scale RES-H_2 hybrid energy system are again summarized below.

5.1 RES - Building

- Annual energy production from the installed RES is approximately 110 MWh.
- Annual energy consumption of the demonstration building is approximately 70 MWh or 131 kWh/m^2/year.
- From an energy perspective, the installed RES are more than adequate to cover the building needs and approximately 30% or produced energy is available for H_2 production.
- Regarding the energy exchange with the PPC, 40% of operation time there is excess of energy in the system and 60% of operation time there is shortage of energy in the system.
- From a power perspective, the installed RES generally can not cover the building needs without applying a load control and balancing scheme.
- Monitoring according to type of load and location is fundamental for proper load control and balancing to satisfy both operational constraints of the system and occupancy requirements.
- Ideal method of load control and balancing would adapt to seasonal variations in order to cater for changes in the building's peak and average loads.

5.2 Electrolyser

- The energy efficiency of the EL is approximately 52%.
- The specific yield of the EL is approximately 6.7 kWh/Nm^3.
- The EL energy consumption and H_2 production rate are successfully regulated by the EMCS through power setpoint signals that are calculated based on the energy balance and/or stored quantity of H_2.
- H_2 losses (venting in EL during and at the end of operation, losses on H_2 compressor etc.) can range from 2% to 12%, resulting in the quantity of stored H_2 to be different than the quantity of produced H_2 by the EL
- Low ambient temperatures have a negative effect on EL performance due to additional energy and time needed for electrolyte warmup.

5.3 Micro-CHP FC

- The total efficiency of the FC is approximately 90% (electrical 47% and thermal 42%).
- The specific yield of the FC is approximately 1.64 kWh_{el}/Nm^3.
- The micro-CHP FC produced power is successfully regulated by the EMCS through power setpoint signals that are calculated based on energy balance and/or stored quantity of H_2.
- H_2 losses (periodic venting during operation, H_2 that does not react etc.) can be as high as 20%.
- Using current H_2 storage capacity (approx. 700 Nm^3) and micro-CHP performance data the following can be calculated:
    - Assuming no energy production from RES and without building load balancing, the micro-CHP can sustain the building operation for approximately 3 days.

- Assuming no energy production from RES and with full building load balancing, the micro-CHP can sustain the building operation for approximately 6 days.

5.4 H_2 Burner

- The specific yield of the H_2 Burner is approximately 1.20 kWh_{th}/Nm^3.
- H_2 Burner and HRS synergistic operation is feasible enabling the integration of H_2 with HVAC systems based on water to air heat exchangers and heat pumps.

5.5 Overall RES-H_2 system

- RES-H_2 hybrid energy system is feasible and a promising technology for the future.
- H_2 system efficiency varies from approximately 15 % to 18 %.
- Using the developed control algorithm the RES-H_2 hybrid energy system can achieve the Zero Energy Building (ZEB) target.
- Using the developed RES-H_2 system CO_2 emissions can be significantly reduced and reach zero.
- Equipment improvements should focus on faster warmup times and lower energy consumption during standby to increase overall system efficiency.
- Equipment improvements should also take into consideration faster response (EL, micro-CHP FC) and synchronization (RES inverters) times for better synergistic operation.
- Off-grid operation of the system can also be feasible using a small battery bank to support the building's critical loads until the micro-CHP FC can start operation and a motorized switch solution to connect and disconnect the system to the PPC when necessary with quick response times.
- The system could be the best practice for isolated areas where the connection to the grid is not feasible or expensive.
- Due to system complexity a ESCOs network is recommended to support the system installation, operation and maintenance.

Under the scope of the H2SusBuild project an intelligent, safe, self-sustained and zero CO_2 emission hybrid energy system to cover electric power, heating and cooling loads (tri-generation) of either residential, commercial and public buildings or districts of buildings has been developed.

The primary energy is harvested from RES and directly used to cover contingent loads, while the excess energy is converted to H_2 to be used as energy storage material and to be further applied as a green fuel to cover the building heating needs through direct combustion or to produce combined heating and electricity by means of fuel cells.

An intelligent power control system that is able to accept variable power supplied from RES, properly control the energy flows to preferentially distribute electrical energy to either cover the primary building's energy demand or to redirect the excess RES energy (when available) to secondary consumptions consisting of the

electrolysis and compression units to allow converting electrical energy to hydrogen and storing the pressurized hydrogen within the storage units has also been developed.

Furthermore, appropriate safety measures have been implemented to guarantee safe operation of the RES-H_2 system through prevention systems, such as suitable ventilation to keep H_2 concentration within safety margins in the building environment, leak detection systems, etc., and fire and explosion protection in case of initiation, such as flame detection systems, flame exclusion systems, etc.

All of the components have been integrated in one operative system, which is efficient, flexible and safe in operation and use. The system can be applied both in residential, commercial and public/institutional buildings.

REFERENCES

Goetzberger A., Hoffmann V.U., “Photovoltaic Solar Energy Generation”, Springer Series in Optical Sciences, 2005, Volume 112/2005, 147-161, DOI: 10.1007/3-540-26628-3_10.

Powalla M., Dimmler B., Schaeffler R., Voorwinden G., Stein U., Mohring H.-D., Kessler F., Hariskos D., “CIGS solar modules: progress in pilot production, new development and applications”, Proceedings of the 19th European Photovoltaic Solar Energy Conference, 2004, p. 1663, Paris, France.

PVGIS @ European Communities 2001-2007, available online at http://re.jrc.ec.europa.eu/pvgis/

Zittel W., Wurster R., “Chapter 3: Productions of Hydrogen, Part 4: Production from electricity by means of electrolysis”, HyWeb: Knowledge – Hydrogen in the Energy Sector, 1996, Ludwig-Bölkow-Systemtechnik GmbH.